

---

Electronic Thesis and Dissertation Repository

---

12-14-2020 10:00 AM

## Electrochemiluminescence of a Di-Boron Complex, Perovskite and Carbon Quantum Dots


Jonathan M. Wong, *The University of Western Ontario*

Supervisor: Ding, Zhifeng, *The University of Western Ontario*

A thesis submitted in partial fulfillment of the requirements for the Master of Science degree in Chemistry

© Jonathan M. Wong 2020

Follow this and additional works at: <https://ir.lib.uwo.ca/etd>

 Part of the [Analytical Chemistry Commons](#), [Materials Chemistry Commons](#), and the [Physical Chemistry Commons](#)

---

### Recommended Citation

Wong, Jonathan M., "Electrochemiluminescence of a Di-Boron Complex, Perovskite and Carbon Quantum Dots" (2020). *Electronic Thesis and Dissertation Repository*. 7534.  
<https://ir.lib.uwo.ca/etd/7534>

This Dissertation/Thesis is brought to you for free and open access by Scholarship@Western. It has been accepted for inclusion in Electronic Thesis and Dissertation Repository by an authorized administrator of Scholarship@Western. For more information, please contact [wlsadmin@uwo.ca](mailto:wlsadmin@uwo.ca).

## Abstract

The electrochemiluminescence (ECL) of three novel materials was explored in this thesis. A di-boron complex exhibiting crystallization-induced blue shift emission was detected utilizing photoluminescence. This phenomenon was successfully observed in the annihilation pathway, resulting in crystallization-induced blue shift ECL. The effects of coreactant and crystallization-induced enhancements were distinguished utilizing two testing systems. Undoped and Mn-doped CsPbCl<sub>3</sub> perovskites were investigated, as the latter exhibits a dual emissive photoluminescence pathway due to host and dopant emission mechanics. It was discovered that the electrochemiluminescence of Mn-doped CsPbCl<sub>3</sub> proceeds through a triplet-triplet annihilation pathway. Furthermore, the relaxation of the electrochemically generated Mn-doped CsPbCl<sub>3</sub> excited state was proposed to relax through a dual emissive pathway (surface states and dopant emission). Finally, a new synthetic method was developed for a green wavelength emitting carbon quantum dots (CQDs) from glucose and phytic acid precursors. Preliminary testing shows promise of CQDs as ECL luminophores.

## Keywords

Electrochemiluminescence (ECL), Photoluminescence, Spectroelectrochemistry, Photoelectrochemistry, Spooling ECL Spectroscopy, Crystallization-Induced Emission, Di-Boron Complex, Mn-doped Perovskites, Carbon Quantum Dots

## Summary for Lay Audience

Electrochemiluminescence (ECL) refers to a light emission process in which electricity is used to generate radical species that can react to form excited state species. It is the relaxation of these excited state species that produces a light emission. This technique can be applied to a wide variety of chemicals, molecules, and even nanomaterials. While there is a high motivation to find bright and highly efficient light emitting compounds and materials, understanding the fundamental processes that lead to formation of excited state species is vital for engineering suitable ECL candidates and developing their applications. In this thesis, three new materials were explored and their interesting light emitting properties examined. A newly synthesized organic compound containing two boron atoms, manganese doped perovskites and carbon nanomaterials formed from glucose were tested for their ECL. Each material is very different and provides a unique lens through which ECL is viewed. In conjunction with different spectroscopy and chemical testing methods, mechanistic insights were obtained in hopes of expanding the applications of these materials towards potential use in light emitting devices and immunoassays.

## Co-Authorship Statement

This thesis includes material from one published manuscript that is presented in Chapter 2. Also included in this thesis is material from one manuscript prepared for submission which is presented in Chapter 3. All work is finalized by ZD.

The manuscript presented in Chapter 2 was published and co-authored by J.M. Wong, R. Zhang, P. Xie, L. Yang, M. Zhang, R. Zhou, R. Wang, Y. Shen, B. Yang, H. Wang, and Z. Ding (*Angew. Chem. Int. Ed.* **2020**, *59*, 17461-17466, DOI: 10.1002/anie.202007588). Photoluminescence quantum efficiencies were measured by PX, MZ, RZ, and RW. DFT calculations were performed by YS and BY. Synthesis of the di-boron complex was performed by RZ, RW and HW. All other photoluminescence, X-ray diffraction, electrochemistry and electrochemiluminescence experiments were performed by JMW (90 %), RZ (5 %) and LY (5 %). Manuscript was prepared by JMW and revised by JMW, RZ, HW and ZD.

The manuscript presented in Chapter 3 was co-authored by, J.M. Wong, J. Xu, R. Zhang, K. Chu, Z. Ding and L. Liu (**2020**, *In Preparation*). Synthesis of the perovskite quantum dots was carried out by JX. ICP-MS, TEM and photoluminescence efficiencies were performed by JX. All other photoluminescence, electrochemistry and electrochemiluminescence experiments were performed by JMW (90%), RZ (5 %) and KC (5 %). JMW wrote and revised the manuscript which was also edited by LL and ZD.

## Acknowledgments

Firstly, I must take this opportunity to thank my supervisor, Dr. Zhifeng Ding, for inspiring me to complete my Masters in his group. He has been a constant source of motivation and guidance throughout the whole process. Without him, I would not be the student I am today. I know that deep down Dr. Ding has his student's best interest at heart. He wants to see us succeed and that has given me the opportunity to achieve the accomplishments that I have throughout my degree. The time and patience that he took to mentor me will never be forgotten and I truly appreciate all that he has done for me. Thank you.

I would also like to thank all the members of the Ding group that I have had the privilege of meeting and working alongside during my fourth-year honor thesis and my Masters. They took the brunt of my daily complaints and were there to support me regardless of the circumstances. To Brandon (come on Liuqing), Kenneth, Fraser, Lina, Mahdi and Dan, I would not have been able to achieve all that I have without your guidance. I also need to thank Ruizhong Zhang, who taught me the fundamentals of research. I am forever in debt to her.

I would not have been able to finish the degree without the support of all my friends that I have made throughout my time here at Western. Thank you to all of you for listening to me rant and watching me die time and time again. To the FLL, Blacquiere, Workentin, Corrigan, Huang and Baines groups, thank you. To Maissa, Andrew, Malin, Susan, Kyle, Justin, Curtis, Karan, Julia, Praveen, Andy, Donghyun and Mengnan you all are amazing. Maissa and Andrew, I am dead.

I also need to thank all my collaborators and the staff at Western that have contributed their time and efforts into my research. I need to thank Mark Workentin, Lijia Liu and Hong-Bo Wang for their patience in dealing with my work style. Without these individuals my thesis would not be complete.

Finally, I would like to thank my friends and family.

*I thank God every day that I have these people in my life. This thesis is dedicated to them.*

# Table of Contents

Abstract.....	ii
Summary for Lay Audience.....	iii
Co-Authorship Statement.....	iv
Acknowledgments.....	v
Table of Contents.....	vi
List of Tables.....	viii
List of Figures.....	ix
List of Appendices.....	xii
List of Abbreviations.....	xiii
Chapter 1.....	1
1 Fundamentals of Electrochemiluminescence (ECL).....	1
1.1 Introduction.....	1
1.2 Ion Annihilation Pathway.....	2
1.3 Benzoyl Peroxide (BPO) Coreactant Pathway.....	3
1.4 Tri-n-propyl amine (TPrA) Coreactant Pathway.....	4
1.5 Scope of Thesis.....	4
1.6 References.....	5
Chapter 2.....	8
2 Revealing Crystallization-induced Blue Shift Emission of a Di-Boron Complex by Enhanced Photoluminescence and Electrochemiluminescence.....	8
2.1 Introduction.....	8
2.2 Photoluminescence and Powder X-ray Diffraction Studies on a New Di-Boron Complex (DBC).....	9
2.3 Electrochemistry and Electrochemiluminescence of the DBC.....	12
2.4 Discussion.....	17

2.5 Experimental .....	20
2.6 References .....	22
Chapter 3 .....	27
3 Discovering the Link between the Electrochemiluminescence and Energy Transfers/Surface States of Mn-Doped CsPbCl <sub>3</sub> Perovskites .....	27
3.1 Introduction .....	27
3.2 Results .....	28
3.3 Electrochemistry and Electrochemiluminescence on the MPQ and UPQ .....	30
3.4 Discussion .....	36
3.5 Experimental .....	41
3.6 References .....	42
Chapter 4 .....	49
4 Carbon Quantum Dots derived from Phytic Acid, Glucose and Phosphoric Acid .....	49
4.1 Introduction .....	49
4.2 Synthesis of Carbon Quantum Dots (CQD) .....	49
4.3 Results and Discussion .....	53
4.4 Experimental .....	57
4.5 References .....	59
Chapter 5 .....	62
5 Conclusions and Future Work .....	62
5.1 Conclusions .....	62
5.2 Future Work and Remarks .....	63
List of Appendices .....	65
Curriculum Vitae .....	73

## List of Tables

Table 4-1. Summary of various pyrolysis trials to synthesize unique carbon quantum dots..	50
Table 4-2. Summary of J-9 dopant ratio synthetic parameter optimization .....	51



## List of Figures

- Figure 2-1. (A) PL spectra of the crystalline DBC film (blue, excited at 532 nm) and a 0.25 mM solution of DBC in acetonitrile (black, excited at 254 nm). The spectra were captured using a 532 nm long pass filter and Oriel spectrograph with an Andor DV429-BC CCD camera. Inset indicates the DBC structure. (B) PL images of recrystallized DBC (leftmost panel), DBC after gradual mechanical grinding (middle three panels), and powder DBC after exposure to acetone vapors for 24 hours (rightmost panel). (C) XRD spectra of DBC recrystallized (blue) and upon grinding (black). Inset is the DBC unit cell. .... 10
- Figure 2-2. CV (red trace, blank CV is dashed line) and corresponding ECL-voltage curve (blue trace) of a 40  $\mu\text{g}$  DBC modified GCE in a 2:1 acetonitrile to  $\text{H}_2\text{O}$  mixture with 0.1 M TBAP as the supporting electrolyte, recorded at a scan rate of 0.1 V/s. Inset displays the LUMO and HOMO DFT images..... 12
- Figure 2-3. Accumulated spectra obtained from the SSECL annihilation pathway (blue trace) with the corresponding curve fitting (dashed line) and SSECL / BPO coreactant route (black trace). Top inset is the annihilation mechanism and the bottom inset is the coreactant mechanism with BPO,  $\text{B} = \text{C}_6\text{H}_5\text{CO}_2^-$ . .... 14
- Figure 2-4. (A) CV (black trace) and ECL-voltage curve (blue trace) of the SSECL / BPO coreactant system utilizing a 40  $\mu\text{g}$  modified GCE and 5 mM BPO in a 2:1 acetonitrile to water solution with 0.1 M TBAP as the supporting electrolyte. (B) CV (black trace) and ECL-voltage curve (orange trace) of the homogenous DBC / BPO coreactant system utilizing a bare GCE and 5 mM BPO in anhydrous acetonitrile with 0.1 M TBAP as the supporting electrolyte. . 16
- Figure 2-5. (A) Spooling ECL spectra of the SSECL / BPO coreactant system obtained by scanning from 0 to -2.0 V at 0.1 V/s with one spectrum taken every 0.25 s, inset shows an overlay of the individual spectra all centering at one wavelength,  $\lambda_{\text{max}} = 630$  nm. (B) Spooling ECL spectra of the homogenous DBC / BPO coreactant system obtained by scanning from 0 to -2.2 V at 0.1 V/s with one spectrum taken every 1 s. Inset indicates an overlay of the individual spectra all centering at one wavelength,  $\lambda_{\text{max}} = 650$  nm. .... 18

Figure 3-1. (A) PL spectra of the undoped CsPbCl<sub>3</sub> perovskite (UPQ - blue trace), doped Mn-CsPbCl<sub>3</sub> perovskite (brown trace) and the MPQ excitation spectrum (red trace). TEM images of (B) MPQ and (C) UPQ. .... 29

Figure 3-2. Cyclic voltammograms and corresponding ECL-voltage curves of GCEs modified with 280 μg MPQ in 0.1 M TBAPF<sub>6</sub> ACN solution (A), 280 μg UPQ in 0.1 M TBAPF<sub>6</sub> ACN solution (B), 280 μg MPQ in 0.1 M TBAPF<sub>6</sub> ACN solution containing 5 mM BPO (C), and 280 μg MPQ in 0.1 M TBAPF<sub>6</sub> ACN solution containing 5 mM BPO (D). The scan rate is 0.1 V/s. Accumulated ECL spectra obtained by pulsing between two potentials for 60 seconds and corresponding curve fitting obtained from MPQ / BPO (E) and UPQ / BPO (F) systems, respectively. .... 31

Figure 3-3. Spooling ECL spectra of the MPQ / BPO coreactant system obtained by scanning from 0 to -2.2 V and back to 0 V at 0.1 V/s with one spectrum taken every 1 s. Inset shows an overlay of the individual spectra all centering at one wavelength  $\lambda_{\text{max}} = 635 \text{ nm}$ . .... 34

Figure 3-4. (A) One ECL spectrum extracted from spooling ECL spectroscopy (Figure 3-3 – scan 21 taken at -2.1 V on the scan towards the cathodic region - red trace) with the corresponding curve fit (black trace) and peak fit (brown and blue trace) for MPQ. (B) *Commission internationale de l'éclairage* chromaticity diagram of the ECL spectrum in (A). .... 35

Figure 3-5. (A) The triplet-triplet annihilation pathway mechanism is outlined for the MPQ. (B) A diagram of the three emissive pathways (1. host, 2. dopant and 3. surface state) that are observed through PL and ECL of the MPQ. .... 37

Figure 4-1. Synthetic procedure to synthesize new CQD from phytic acid, glucose and phosphoric acid precursors. .... 52

Figure 4-2. Fluorescence images obtained of (A) Glucose, (B) Phytic Acid, (C) Purified CQD dispersed in water (0.1 g/mL), under a 254 nm UV lamp and (D) Purified CQD dispersed in water (0.1 g/mL) under broad daylight. (E) PL spectra of the CQD dispersed in water (0.1 g/mL) excited at varying wavelengths from 300 to 420 nm. .... 53

Figure 4-3. (A) PL spectra depicting the pH dependent nature of the CQD emission upon photoexcitation at 415 nm (0.1 g/mL). (B) Maximum PL intensity versus pH of the newly synthesized CQD taken at  $\lambda_{\text{Emission}} = 515$  nm upon photoexcitation at 415 nm (0.1 g/mL)... 54

Figure 4-4. (A) Cyclic voltammogram of the CQD – red trace, blank – dotted line, and the corresponding ECL voltage curve – blue trace upon scanning towards the cathodic region. (B) Cyclic voltammogram of the CQD – red trace, blank – dotted line, and the corresponding ECL voltage curve – blue trace upon scanning towards the anodic region..... 55

Figure 4-5. Cyclic voltammogram of the CQD – red trace and corresponding ECL-voltage curve (blue trace) of a 10 mg modified GCE in 1:1 water:acetonitrile solution with 0.1 M TBAP as the supporting electrode with (A) 5 mM BPO and (B) 20 mM TPrA as the coreactant. ... 56

## List of Appendices

Appendix A: Reproduction permission for the paper “Revealing Crystallization Induced Blue Shift Emission of a Di-Boron Complex by Enhanced Photoluminescence and Electrochemiluminescence” .....	65
Appendix B: Supporting Information for the paper “Revealing Crystallization Induced Blue Shift Emission of a Di-Boron Complex by Enhanced Photoluminescence and Electrochemiluminescence” .....	70

## List of Abbreviations

AIE	Aggregation-Induced Emission
AIECL	Aggregation-Induced Electrochemiluminescence
BPO	Benzoyl Peroxide
BODIPY	Boron dipyrromethene
CCD	Charge-coupled Device
CE	Counter Electrode
CIBS-ECL	Crystallization-Induced Blue Shift Electrochemiluminescence
CIE	Crystallization-Induced Emission
CV	Cyclic Voltammetry or Cyclic Voltammogram
CQD	Carbon Quantum Dot
CQDs	Carbon Quantum Dots
DBC	Di-boron Complex
DFT	Density Functional Theory
ECL	Electrochemiluminescence
Em	Emission
Ex	Excitation
Fc	Ferrocene
Fc <sup>+</sup>	Ferrocenium Cation
HOMO	Highest Occupied Molecular Orbital

ICP-MS	Inductively Coupled Plasma - Mass Spectrometry
LUMO	Lowest Unoccupied Molecular Orbital
MPQ	Manganese Doped CsPbCl <sub>3</sub> Perovskite Quantum Dot
Ox	Oxidation
PL	Photoluminescence
PMT	Photomultiplier Tube
RE	Reference Electrode
Red	Reduction
RIR	Restriction of Intramolecular Rotation
[Ru(bpy) <sub>3</sub> ] <sup>2+</sup>	Tris(2,2'-bipyridine)ruthenium (II)
SCE	Saturated Calomel Electrode
SSECL	Solid State Electrochemiluminescence
TBAP	Tetra- <i>n</i> -butylammonium Perchlorate
TBAPF <sub>6</sub>	Tetra- <i>n</i> -butylammonium Hexafluorophosphate
TPrA	Tri- <i>n</i> -propylamine
UPQ	Undoped CsPbCl <sub>3</sub> Perovskite Quantum Dot
UV	Ultraviolet
Vis	Visible
WE	Working Electrode
XRD	X-ray Diffraction



## Chapter 1

# 1 Fundamentals of Electrochemiluminescence (ECL)

## 1.1 Introduction

Electrochemiluminescence or electrogenerated chemiluminescence (ECL) is a light emitting process that capitalizes on the redox properties of luminophores.<sup>1-2</sup> The radical species electrogenerated in the vicinity of an electrode can undergo further electron transfer reactions to produce excited state species which can relax to emit light.<sup>3</sup> Intrinsically, this elegant light emitting technique circumvents the need for an external light source and as a result a detection limit as low as femtomolar can be obtained.<sup>4-5</sup> ECL has found its use in bioanalytical immunoassays for antigen detection which exploit the extreme sensitivity of this technique. Since its development, Bard and coworkers have pioneered and paved the way for current developments in the field.<sup>6-8</sup> Most notably their detailed work on the ECL of tris(2,2'-bipyridine)ruthenium (II),  $[\text{Ru}(\text{bpy})_3]^{2+}$ , remains the standard for efficiency determination of new luminophores.<sup>9</sup>

Although the applications of ECL in bioanalytical assays have been well established, the ECL mechanisms are currently being applied towards procuring light emitting devices.<sup>10-11</sup> A wide array of nanomaterials, clusters and novel organic compounds have already been shown as bright ECL luminophores.<sup>12-16</sup> As such, with constant new developments to materials research, their application in ECL has yet to be uncovered, developed, and studied.

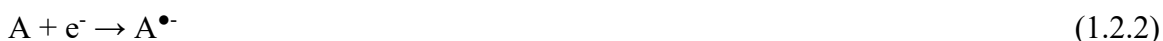
One item that must be addressed when talking about ECL is photoluminescence or PL, which encapsulates and probes both phosphorescence and fluorescence of the luminophore. PL studies remain as the most widespread opto-physical measurements performed, easily determining the quantum efficiency or quantum yield of the light emitting material. As a result, mechanisms involving photoinduced light emission are often well studied or elucidated. This provides an excellent foundation for ECL studies to build upon in further understanding the electrochemically induced light emission pathways, as spectral properties can be compared. The comparison between ECL and PL spectral



properties is integral in understanding and elucidating the ECL mechanism.<sup>3</sup> This theme will be revisited consistently throughout each chapter in this thesis, as PL is vital in fully understanding the ECL phenomenon that is observed experimentally. High ECL efficiencies are of course, always lucrative in the testing of new compounds and nanomaterials. However, this is secondary in comprehending the fundamental ECL mechanisms and in seeking to expand this field. Therefore, in hopes of further expanding the field of ECL, understanding the fundamental light emission pathways must be addressed.

## 1.2 Ion Annihilation Pathway

ECL occurs primarily through two different pathways with the first being the annihilation pathway or ion annihilation pathway. If the ECL active luminophore possesses a HOMO and LUMO that can be probed in the solvent potential window, observance of the annihilation of radically generated ions may be possible.<sup>17</sup> Oxidation of the luminophore occurs upon scanning towards the anodic region, producing the radical cation species (Eq. 1.2.1). Then as the potential is scanned towards the cathodic region, the radical anion species can be electrogenerated near the vicinity of the electrode surface in solution (Eq. 1.2.2). If the electrogenerated species meet in solution, an electron transfer reaction can occur between the two, which results in the formation of an excited state species and ground state species, this is also known as ion annihilation (Eq. 1.2.3).<sup>18</sup> The excited state species then relaxes to emit light at a given wavelength (Eq. 1.2.4).<sup>19</sup>

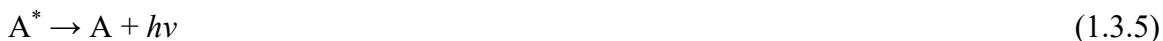


However, it must be noted that two key factors influence the likelihood of observing ECL. Firstly, the stability of the electrogenerated radical species is important as the radical cation generated at the anodic region must survive the scan until the radical anion species

is generated.<sup>3</sup> Secondly, favorable electron transfer processes must occur between the two species in order to produce ECL. If either of the two criteria is lacking, ECL in the annihilation pathway will not occur.<sup>2</sup>

### 1.3 Benzoyl Peroxide (BPO) Coreactant Pathway

Since the inception of ECL, the coreactant pathway has played an important role in enhancing the emission of the luminophore. Often, the ion annihilation pathway results in a low ECL emission, largely due to the instability of the radically generated cation and anion species. Therefore, in an aim to enforce ECL emission, a coreactant can be added to encourage the formation of excited state species. The bulk of this thesis focuses on the ECL obtained through the generation of the luminophore's radical anion species (Eq. 1.3.1). A compatible coreactant is benzoyl peroxide (BPO) which upon reduction cleaves to generate the benzoate radical (Eq. 1.3.2 & 1.3.3).<sup>18</sup> This species is extremely oxidizing and can extract an electron from the HOMO of the electrogenerated radical anion of the luminophore (Eq. 1.3.4).<sup>20-21</sup> This results in the formation of the excited state species, which can relax to emit light (Eq. 1.3.5). It is crucial to note that the electron transfer processes can result in several different outcomes. However, in order to observe light, the excited state species must be generated. Therefore, the extraction of an electron from the HOMO of the radical anion species is necessary for ECL to occur in this pathway.<sup>3, 22</sup>



## 1.4 Tri-n-propyl amine (TPrA) Coreactant Pathway

The second coreactant pathway, which is utilized when probing the ECL of the electrogenerated radical cation species, often uses tri-n-propyl amine (TPrA). The TPrA pathway has been widely studied by Bard and coworkers and capitalizes on the highly reducing TPrA<sup>•</sup> species ((CH<sub>3</sub>CH<sub>2</sub>CH<sub>2</sub>)<sub>2</sub>NC<sup>•</sup>HCH<sub>2</sub>CH<sub>3</sub>).<sup>9,23</sup> The radical lies on one of the carbon atoms bound to the central nitrogen.<sup>24-25</sup> As a result, this species can donate an electron to the LUMO of the electrogenerated radical cation (Eq. 1.4.1 - 1.4.3). This leads to the production of the excited state species which can then undergo relaxation to emit light at a specified wavelength (Eq. 1.4.4).<sup>26</sup> In a similar manner to the BPO coreactant pathway, electron transfer reactions can result in a many different outcomes, but production of the excited state species must occur to observe ECL.<sup>2</sup>



## 1.5 Scope of Thesis

The scope of this thesis aims to address the ECL of three novel materials and/or compounds, a new organic di-boron complex, manganese doped cesium lead halide perovskite and carbon quantum dots in Chapters 2-4. In each of the chapters, we hope to explain and develop the emissive pathway of ECL and utilize spectroscopy to ascertain the corresponding ECL mechanisms. Furthermore, the conjunction of new materials and optoelectronic properties such as crystallization-induced emission and transition metal doping into nanomaterials will be addressed as it pertains to ECL. Chapter 5 provides a summary and perspective into future work.

## 1.6 References

1. Hesari, M.; Ding, Z., Review—Electrogenerated Chemiluminescence: Light Years Ahead. *J. Electrochem. Soc.* **2016**, *163* (4), H3116-H3131.
2. Bard, A. J., *Electrogenerated Chemiluminescence*. 1 ed.; Marcel Dekker, Inc.: New York, NW 10016, U.S.A., 2004; p 16.
3. Richter, M. M., Electrochemiluminescence (ECL). *Chem. Rev.* **2004**, *104* (6), 3003-3036.
4. Wang, D.; Li, Y.; Lin, Z.; Qiu, B.; Guo, L., Surface-Enhanced Electrochemiluminescence of Ru@SiO<sub>2</sub> for Ultrasensitive Detection of Carcinoembryonic Antigen. *Anal. Chem.* **2015**, *87* (12), 5966-5972.
5. Lu, J.; Wu, L.; Hu, Y.; Wang, S.; Guo, Z., Ultrasensitive Faraday Cage-type Electrochemiluminescence Assay for Femtomolar miRNA-141 via Graphene Oxide and Hybridization Chain Reaction-assisted Cascade Amplification. *Biosens. Bioelectron.* **2018**, *109*, 13-19.
6. Cao, W. D.; Zhang, X. H.; Bard, A. J., Electrogenerated Chemiluminescence. 75. Electrochemistry and ECL of 9,10-bis(2-naphthyl)anthracene. *J. Electroanal. Chem.* **2004**, *566* (2), 409-413.
7. Tokel, N. E.; Bard, A. J., Electrogenerated Chemiluminescence. IX. Electrochemistry and Emission from Systems Containing Tris(2,2'-bipyridine)ruthenium(II) dichloride. *J. Am. Chem. Soc.* **1972**, *94* (8), 2862-2863.
8. Tokel, N. E.; Keszthelyi, C. P.; Bard, A. J., Electrogenerated chemiluminescence. X.  $\alpha$ ,  $\beta$ ,  $\gamma$ ,  $\delta$ -Tetraphenylporphine Chemiluminescence. *J. Am. Chem. Soc.* **1972**, *94* (14), 4872-4877.
9. Miao, W.; Choi, J.-P.; Bard, A. J., Electrogenerated Chemiluminescence 69: The Tris(2,2'-bipyridine)ruthenium(II), (Ru(bpy)<sub>3</sub><sup>2+</sup>)/Tri-n-propylamine (TPrA)

- System Revisited - A New Route Involving TPrA<sup>+</sup> Cation Radicals. *J. Am. Chem. Soc.* **2002**, *124* (48), 14478-14485.
10. Pei, Q.; Heeger, A. J., Operating Mechanism of Light-emitting Electrochemical Cells. *Nat. Mater.* **2008**, *7* (3), 167-167.
  11. Buda, M.; Kalyuzhny, G.; Bard, A. J., Thin-Film Solid-State Electroluminescent Devices Based On Tris(2,2'-bipyridine)ruthenium(II) Complexes. *J. Am. Chem. Soc.* **2002**, *124* (21), 6090-6098.
  12. Swanick, K. N.; Ladouceur, S.; Zysman-Colman, E.; Ding, Z. F., Self-Enhanced Electrochemiluminescence of an Iridium(III) Complex: Mechanistic Insight. *Angew. Chem. Int. Ed.* **2012**, *51* (44), 11079-11082.
  13. Swanick, K. N.; Hesari, M.; Workentin, M. S.; Ding, Z., Interrogating Near-Infrared Electrogenerated Chemiluminescence of Au<sub>25</sub>(SC<sub>2</sub>H<sub>4</sub>Ph)<sub>18</sub><sup>+</sup> Clusters. *J. Am. Chem. Soc.* **2012**, *134* (37), 15205-15208.
  14. Carrara, S.; Aliprandi, A.; Hogan, C. F.; De Cola, L., Aggregation-Induced Electrochemiluminescence of Platinum(II) Complexes. *J. Am. Chem. Soc.* **2017**, *139* (41), 14605-14610.
  15. Ding, Z.; Quinn, B. M.; Haram, S. K.; Pell, L. E.; Korgel, B. A.; Bard, A. J., Electrochemistry and Electrogenerated Chemiluminescence from Silicon Nanocrystal Quantum Dots. *Science* **2002**, *296* (5571), 1293-1297.
  16. Nepomnyashchii, A. B.; Bard, A. J., Electrochemistry and Electrogenerated Chemiluminescence of BODIPY Dyes. *Acc. Chem. Res.* **2012**, *45* (11), 1844-1853.
  17. Hercules, D. M., Chemiluminescence Resulting from Electrochemically Generated Species. *Science* **1964**, *145* (3634), 808-809.
  18. Chandross, E. A.; Sonntag, F. I., Chemiluminescent Electron-Transfer Reactions of Radical Anions. *J. Am. Chem. Soc.* **1966**, *88* (6), 1089-1096.

19. Bezman, R.; Faulkner, L. R., Mechanisms of Chemiluminescent Electron-transfer Reactions. V. Absolute Measurements of Rubrene Luminescence in Benzonitrile and N,N-dimethylformamide. *J. Am. Chem. Soc.* **1972**, *94* (18), 6324-6330.
20. Choi, J.-P.; Wong, K.-T.; Chen, Y.-M.; Yu, J.-K.; Chou, P.-T.; Bard, A. J., Electrogenenerated Chemiluminescence. 76. Excited Singlet State Emission vs Excimer Emission in Ter(9,9-diarylfluorene)s. *J. Phys. Chem. B* **2003**, *107* (51), 14407-14413.
21. Santa Cruz, T. D.; Akins, D. L.; Birke, R. L., Chemiluminescence and Energy Transfer in Systems of Electrogenenerated Aromatic Anions and Benzoyl Peroxide. *J. Am. Chem. Soc.* **1976**, *98* (7), 1677-1682.
22. Omer, K. M.; Ku, S.-Y.; Wong, K.-T.; Bard, A. J., Green Electrogenenerated Chemiluminescence of Highly Fluorescent Benzothiadiazole and Fluorene Derivatives. *J. Am. Chem. Soc.* **2009**, *131* (30), 10733-10741.
23. Leland, J. K., Electrogenenerated Chemiluminescence: An Oxidative-Reduction Type ECL Reaction Sequence Using Tripropyl Amine. *J. Electrochem. Soc.* **1990**, *137* (10), 3127.
24. Mann, C. K., Cyclic Stationary Electrode Voltammetry of Some Aliphatic Amines. *Anal. Chem.* **1964**, *36* (13), 2424-2426.
25. Smith, P. J.; Mann, C. K., Electrochemical Dealkylation of Aliphatic Amines. *The J. Org. Chem.* **1969**, *34* (6), 1821-1826.
26. Zu, Y.; Bard, A. J., Electrogenenerated Chemiluminescence. 66. The Role of Direct Coreactant Oxidation in the Ruthenium Tris(2,2')bipyridyl/Tripropylamine System and the Effect of Halide Ions on the Emission Intensity. *Anal. Chem.* **2000**, *72* (14), 3223-3232.

## Chapter 2

# 2 Revealing Crystallization-induced Blue Shift Emission of a Di-Boron Complex by Enhanced Photoluminescence and Electrochemiluminescence<sup>†</sup>

## 2.1 Introduction

Highly efficient luminescent boron complexes, most notably the single boron dipyrromethene (BODIPY) dyes, are a class of organic luminophores possessing highly tunable emission wavelengths achieved through simple structure modifications.<sup>1-4</sup> However, the solid-state emission of these tetracoordinate boron BODIPY dyes often suffers due to their planar nature which undergoes efficient  $\pi$ -stacking upon aggregation or crystallization.<sup>5-6</sup> Strong  $\pi$ - $\pi$  interaction between planar molecules often produces excimer species, which favors non-radiative emission of energy through charge transfer.<sup>6</sup> It is interesting though that Tang and co-workers observed an emission enhancement phenomenon of silole molecules containing rotary ligands upon aggregating and crystallizing.<sup>7-8</sup> In solution, freely rotating ligands offer an opportune means by which energy is lost non-radiatively through intramolecular motions.<sup>8</sup> Restriction of intramolecular rotation (RIR) of freely rotating ligands upon aggregation prevented this energy loss and enforced a bright emission as radiative relaxation was favored, developing the concept of aggregation induced emission (AIE).<sup>9-10</sup> Crystallization induced emission (CIE) procures a similar effect as AIE by means of restricting intramolecular rotation through lattice formation.<sup>11-13</sup> As such, tetracoordinate boron luminophores are optimal candidates to realize solid-state emission enhancement (through AIE and/or CIE), broadening their versatility for applications in both the solution and solid state.

One facile method capable of comparing the viability of a luminophore in both solution and solid state is studying the electrochemiluminescence or electrogenerated

---

<sup>†</sup> This work is published in J.M. Wong, R. Zhang, P. Xie, L. Yang, M. Zhang, R. Zhou, R. Wang, Y. Shen, B. Yang, H. Wang, and Z. Ding (*Angew. Chem. Int. Ed.* **2020**, *59*, 17461-17466, DOI: 10.1002/anie.202007588). Reproduced by permission of John Wiley and Sons. See Appendix A.

chemiluminescence (ECL).<sup>14-22</sup> This is an elegant light emitting process that capitalizes on the luminophore's redox properties, with which nanomaterials, quantum dots, metal clusters and various molecules have been investigated.<sup>23-25</sup> Its practical applications are seen in bioanalytical immunoassays and in light emitting diodes.<sup>26-28</sup> Precious metal complexes are conventionally employed as ECL luminophores and as a result, active research is pursued to yield low cost and bright emitting alternatives.<sup>29-30</sup> Mechanistic studies reveal the fundamental nature of ECL, a crucial aspect in reaction proposals that are often overlooked.<sup>22</sup> This is especially important when seeking to understand the implications of solid-state emission enhancement, which should be compared to solution ECL. The investigation on the solution ECL of BODIPY-based dyes including dimeric and trimeric species was previously performed.<sup>4, 20</sup> However, these studies did not probe nor find solid-state emission enhancement. Furthermore, there are only a few published works outlining aggregation-induced ECL (AIECL) in dispersions of Pt and Ir complexes.<sup>31-33</sup> Only recently has AIECL of carboranyl and siloles been reported.<sup>34-35</sup> However even outside the notions of AIECL, very few studies precisely compare the nature of both solid-state and solution ECL. Therefore, this work seeks to unambiguously explain CIE for ECL enhancement through the comparison of crystalline and solution states. In conjunction with photoluminescence (PL) studies, we shed light on the ability to elucidate RIR and further confirm CIE through electro/photo-induced spectroscopic techniques. We capitalize on the solid-solution interfacial electrochemistry to study a newly synthesized di-boron complex (DBC).

## 2.2 Photoluminescence and Powder X-ray Diffraction Studies on a New Di-Boron Complex (DBC)

PL measurements were first performed on the DBC (shown in the inset of Figure 2-1A) in the crystalline state and in solution. Figure 2-1A shows the PL spectra of the recrystallized DBC film (blue) and of a 0.25 mM DBC in acetonitrile (black).



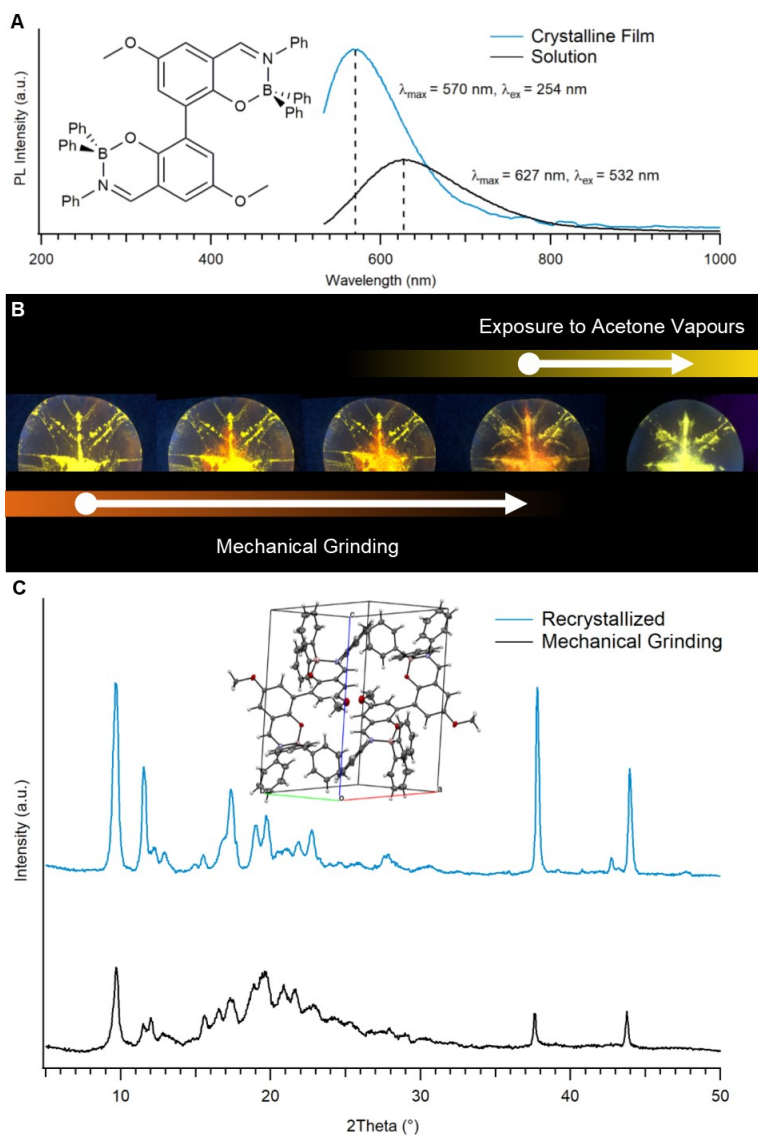


**Figure 2-1.** (A) PL spectra of the crystalline DBC film (blue, excited at 532 nm) and a 0.25 mM solution of DBC in acetonitrile (black, excited at 254 nm). The spectra were captured using a 532 nm long pass filter and Oriel spectrograph with an Andor DV429-BC CCD camera. Inset indicates the DBC structure. (B) PL images of recrystallized DBC (leftmost panel), DBC after gradual mechanical grinding (middle three panels), and powder DBC after exposure to acetone vapors for 24 hours (rightmost panel). (C) XRD spectra of DBC recrystallized (blue) and upon grinding (black). Inset is the DBC unit cell.

The corresponding excitation-independent emission peak wavelengths were found to be 570 nm and 627 nm, respectively. An interesting 57 nm blue shift upon reversion of

the solution dispersed DBC to the crystalline state was discovered. This diverges from the normative redshift emission, often observed from organic luminophores transitioning from the solution to solid-state.<sup>36</sup> The blue shift is further illustrated by the luminescence photographs in Figure 2-1B. Upon mechanical grinding of the crystalline DBC, the luminescence changes from a yellow (shorter wavelength) to orange/red color (longer wavelength). Moreover, exposing the DBC powder with orange/red luminescence to acetone vapors for 24 hours allowed for recrystallization to the yellow-colored luminous crystals (two right luminescence images in Figure 2-1B). The X-ray diffraction spectra shown in Figure 2-1C depict well the crystallinity changes before and after mechanical grinding. It is evident that the luminescent color changes are the result of the switch between crystalline and amorphous-like powder morphology and that the crystallinity has induced a blue shifted emission, a phenomenon discovered by Tang's group on (4-biphenyl) phenyldibenzofulvene, metal- and heavy atom-free aromatic acids and esters.<sup>11-12</sup> In fact, the crystallization-induced blue shift (CIBS) emission observed in the crystalline state PL is a direct consequence of RIR. Restriction of rotamers such as the phenyl substituents off the nitrogen in the DBC, which led to non-radiative relaxation in solution, now enforce light emission. The efficient packing of the DBC demonstrated in the unit cell (inset of Figure 2-1C) prevents rotation and out-of-plane bending modes (both means of non-radiative energy loss), leading to a higher energy emission wavelength. The blue shift is very similar to that of typical AIE-active molecules such as 9,10-distyrylanthracene in both solvents and aggregates, as well as others.<sup>13, 37-38</sup>

More interestingly, emission intensity enhancement was also observed for the DBC crystalline solid compared to that of the solution phase. The absolute PL quantum yield ( $\Phi_{\text{PL}}$ ) for the DBC in crystalline solid and acetonitrile was determined to be 21.5 % and 6.6 %, respectively. The nearly 4 times increase in the PL efficiency clearly illustrates not only a conserved but enhanced emission as individual DBC molecules undergo lattice packing. The various possibilities in structural modifications that can arise from simply increasing the number of boron atoms aids us in engineering a bright emitting luminophore that resists quenching upon reversion to solid state. Thus, the DBC offers an interesting prospect, to realize two CIE characteristics in ECL. Here, we report for the first time CIE-ECL and the corresponding CIBS-ECL.

## 2.3 Electrochemistry and Electrochemiluminescence of the DBC

Solid-state ECL (SSECL) was first studied by means of a modified 3 mm diameter glass carbon electrode (GCE) with a 40  $\mu\text{g}$  loading of the DBC by drop casting a 0.25 mM stock solution prepared with acetonitrile. The filmed electrode was left to dry overnight in air. SSECL was conducted in a 2:1 acetonitrile:water mixture which prevented the film's dissolution. Tetrabutylammonium perchlorate (TBAP) was added at 0.1 M as the supporting electrolyte. Cyclic voltammetry (CV) was carried out by scanning the potential between -1.7 to 2.0 V vs SCE at a scan rate of 0.1 V/s.

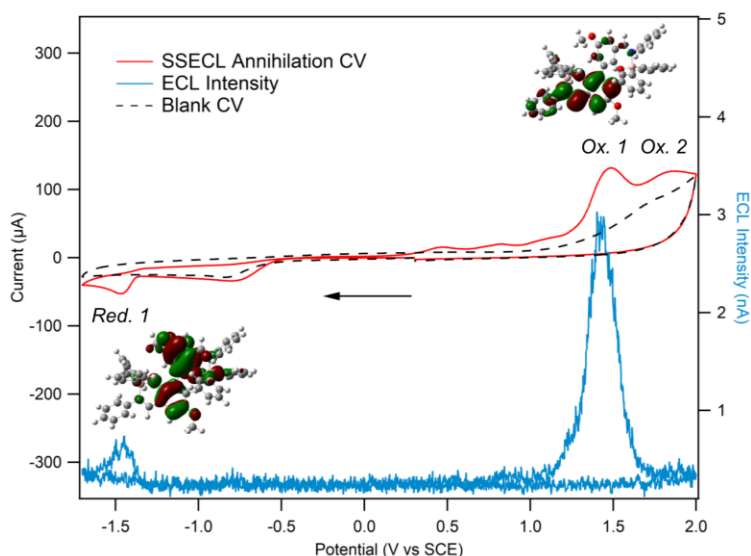


**Figure 2-2.** CV (red trace, blank CV is dashed line) and corresponding ECL-voltage curve (blue trace) of a 40  $\mu\text{g}$  DBC modified GCE in a 2:1 acetonitrile to  $\text{H}_2\text{O}$  mixture with 0.1 M TBAP as the supporting electrolyte, recorded at a scan rate of 0.1 V/s. Inset displays the LUMO and HOMO DFT images.

Besides the minor reduction peak of the residual oxygen at -0.75 V, the CV in Figure 2-2 (red trace) shows one broad reduction peak at  $E_{\text{red}} = -1.43$  V and two oxidation peaks at  $E_{\text{ox}} = 1.48$  V and 1.83 V. All potentials were referenced against the saturated calomel electrode (SCE) by means of an internal ferrocene/ferrocenium ( $\text{Fc}/\text{Fc}^+$ ) standard

taken at 0.424 V vs SCE.<sup>39</sup> The electrochemical potential difference between the first oxidation and reduction peaks, 2.85 V, agrees well with that of the HOMO-LUMO gap of 3.0 eV found through DFT (Table B1 in Appendix B). As illustrated in the molecular orbitals (Figure 2-2), oxidation of the DBC from the HOMO occurs primarily from the  $\pi$ -conjugated backbone, while the reduction arises from the injection of electrons to the LUMO, principally at the N-O chelate moiety. SSECL from the annihilation of electrogenerated radical DBC species was observed in both the cathodic and anodic regions (blue trace in Figure 2-2). The onset potential of SSECL in both the cathodic and anodic regions correspond well to the first oxidation and first reduction reactions of the DBC. As a result, the electrogenerated radical cation and anion meet, annihilating to the ground state and excited state, which upon relaxation emits light. Sufficient lifetimes and favorable electron transfer between species are the two criteria governing the observation of light emission. The SSECL found in the anodic region is substantially brighter than that of the cathodic region. This discrepancy indicates the high stability of the radical anion,  $\text{DBC}^{\bullet-}$ , surviving through the scan process towards the anodic region to react with the radical cation species,  $\text{DBC}^{\bullet+}$ , being generated at 1.48 V. Meanwhile,  $\text{DBC}^{\bullet+}$  does not exhibit such stability as only a small fraction survives the scan towards the cathodic region producing SSECL of lower intensity. As the potential is scanned further positive, no ECL is generated at the second oxidation potential as likely all  $\text{DBC}^{\bullet-}$  species in the film have been depleted and  $\text{DBC}^{2+}$  does not react with DBC to regenerate  $\text{DBC}^{\bullet-}$  which prevents excited state production.

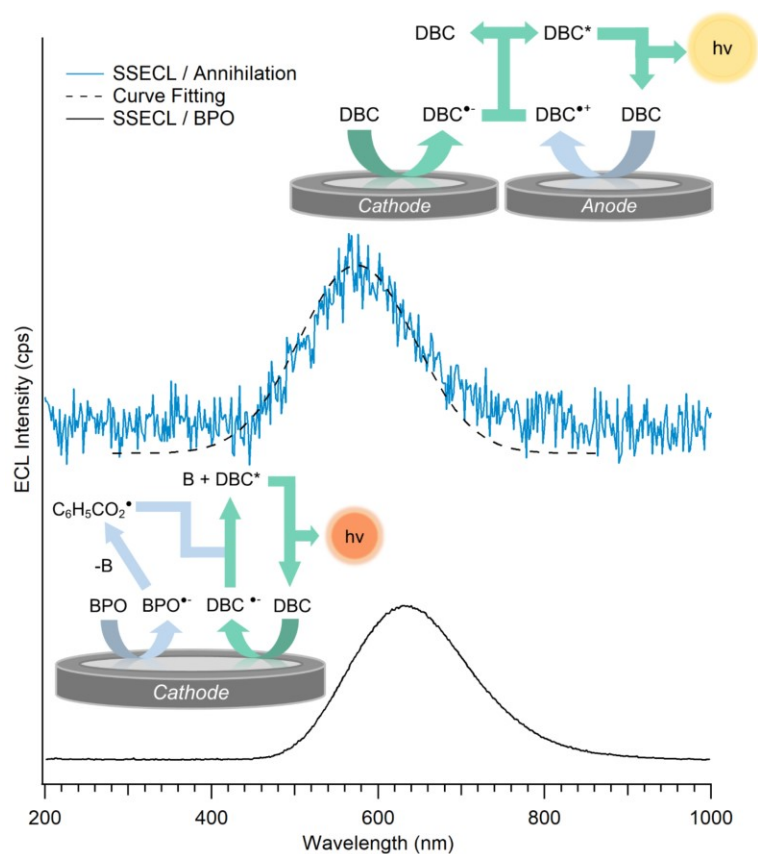


**Figure 2-3.** Accumulated spectra obtained from the SSECL annihilation pathway (blue trace) with the corresponding curve fitting (dashed line) and SSECL / BPO coreactant route (black trace). Top inset is the annihilation mechanism and the bottom inset is the coreactant mechanism with BPO, B =  $C_6H_5CO_2^-$ .

A spectrum was obtained of the SSECL generated from the annihilation of DBC radicals by pulsing between -1.70 and 2.00 V (blue trace in Figure 2-3,  $\lambda_{max} = 570$  nm). In fact, pulsing between the two potentials reduces the time required for the electrogenerated DBC radicals to meet, encouraging ECL emission. This peak wavelength mimics that of the solid-state PL spectrum shown in Figure 2-1A (black trace,  $\lambda_{max} = 570$  nm). Since excited state species produce distinct emissions, spectral data provides compelling evidence to discern between CIE/AIE effects and increased concentration enhancements encountered in SSECL. For this reason, the light-emitting species stemming from photoexcitation is likely the same as that produced by the annihilation of electrogenerated radicals. The mechanism for SSECL from the annihilation is outlined in the top inset of

Figure 2-3. The production of the radical  $\text{DBC}^{\bullet}$  occurs at -1.43 V, which remain in the film. By scanning towards the anodic region, the radical cation species  $\text{DBC}^{\bullet+}$  is generated, immediately undergoing an electron transfer reaction with  $\text{DBC}^{\bullet}$ . This produces the excited state  $\text{DBC}^*$  that relaxes to emit light.

This is the first example of crystallization-induced blue shift emission obtained through ECL (CIBS-ECL). Due to the nature of SSECL, the production of radical anion and cation species occurs within the DBC film in the vicinity of the electrode surface. The electrogenerated DBC radicals are well confined in the crystal lattice. The observation of CIBS-ECL is therefore quite reasonable, as species annihilated are well affected by RIR. The ECL efficiency ( $\Phi_{\text{ECL}}$ ) was calculated relative to 0.25 mM  $[\text{Ru}(\text{bpy})_3]^{2+}$  in solution and found to be 8.5 % in the annihilation pathway utilizing the equation B1 in Appendix B. It is understandable that utilizing a solid-solution system acquires limitations with the film's structure.<sup>14</sup> Therefore, the SSECL intensity is not easily optimized. The congruency between the observed electrochemical features, DFT calculations and identical emission  $\lambda_{\text{max}}$  between ECL and PL, confirms the notion of CIBS-ECL. To probe the light emission from individual DBC species in the absence of any crystalline phases, a secondary system was studied (solution ECL). A traditional bare GCE in a 0.25 mM DBC acetonitrile solution with 0.1 M TBAP as the supporting electrolyte was used. The CV exhibits a similar profile to that of the DBC film, though no ECL was detected (Figure B2 in Appendix B). The lack of ECL arises from the short lifetimes of the electrogenerated radical species in solution. This further strengthens the notion of DBC as a luminophore in solid state devices as the electrogenerated radical species in the crystalline film are more stable than that of solution.

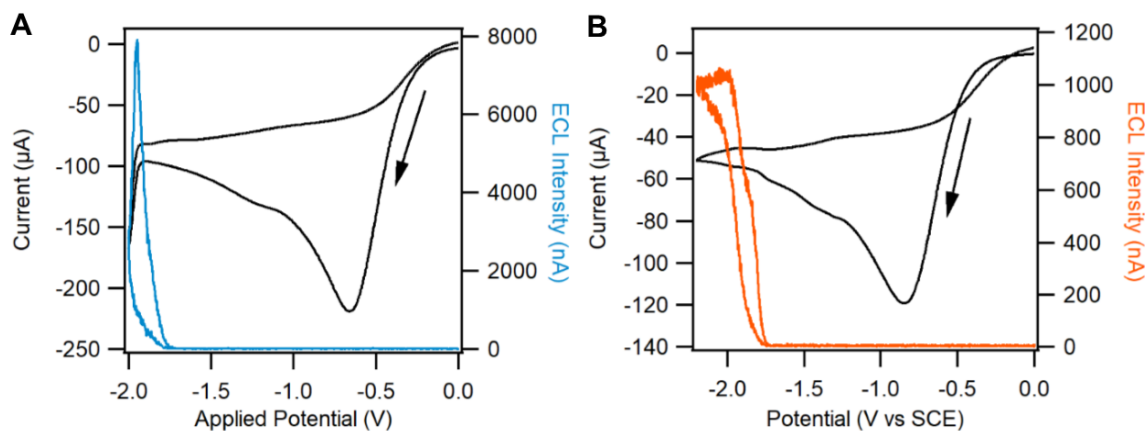


**Figure 2-4.** (A) CV (black trace) and ECL-voltage curve (blue trace) of the SSECL / BPO coreactant system utilizing a 40  $\mu\text{g}$  modified GCE and 5 mM BPO in a 2:1 acetonitrile to water solution with 0.1 M TBAP as the supporting electrolyte. (B) CV (black trace) and ECL-voltage curve (orange trace) of the homogenous DBC / BPO coreactant system utilizing a bare GCE and 5 mM BPO in anhydrous acetonitrile with 0.1 M TBAP as the supporting electrolyte.

Adding a coreactant such as benzoyl peroxide (BPO) often enhances the ECL due to the strong oxidizing nature of the electrogenerated benzoate radicals. Upon the addition of 5 mM BPO a substantial increase in the SSECL intensity was observed (Figure 2-4A). In the CV (black trace), BPO reduction occurs at -0.66 V. By scanning further negative, at an onset potential of -1.73 V, SSECL emission is produced. This matches well with the reduction potential of the DBC species to  $\text{DBC}^{\bullet-}$ . A 2600 times increase in ECL intensity, represented by a photocurrent of 8  $\mu\text{A}$  from a photomultiplier tube (PMT) biased at -750 V, was obtained compared to that in the annihilation pathway (3 nA in Figure 2-2A). This is a very strong ECL emission. Due to the bright luminescence, the accumulated spectrum of the SSECL / BPO coreactant system was obtained by scanning the potential from 0.0 to -2.0 V which resulted in an emission with a  $\lambda_{\text{max}} = 630 \text{ nm}$  (black trace in Figure 2-3). It is striking that although strong ECL enhancement was obtained, a red shift in the wavelength of light emitted was observed in comparison to that in the annihilation pathway (blue trace in Figure 2-3). Furthermore, the SSECL / BPO spectrum is nearly identical to that of the solution PL spectrum ( $\lambda_{\text{max}} = 630 \text{ nm}$  as seen in the black trace of Figure 2-1A). To probe further the ECL from DBC / BPO in the absence of crystalline phases, 5 mM BPO was

added to the homogenous 0.25 mM DBC solution system and CV was performed (Figure 2-4B). ECL was produced in the cathodic region to 1  $\mu\text{A}$  in intensity, nearly 8 times lower than that of the SSECL / BPO system (Figure 2-4A). The  $\Phi_{\text{ECL}}$  of both the film and solution DBC was compared to the 0.25 mM  $[\text{Ru}(\text{bpy})_3]^{2+}$  / BPO system. The  $\Phi_{\text{ECL}}$  of the SSECL / BPO system is 4.7 %, where a more than 5 times increase is observed in the solid-state relative to solution ECL / BPO (0.85 %). It should be noted that both the addition of coreactant and RIR are light enhancing factors. The increase in  $\Phi_{\text{ECL}}$  of the SSECL / BPO system with respect to the solution ECL / BPO system alludes towards contributions from RIR. Filmed electrodes produce vastly increased current values due to the introduction of a solid interface. This exacerbates the charge contribution in the efficiency calculation of the SSECL / BPO system (refer to equation B1 in the Appendix B). Therefore, an intrinsic prejudice exists, negatively skewing the observed efficiency in contrast to the solution  $[\text{Ru}(\text{bpy})_3]^{2+}$  / BPO system.

## 2.4 Discussion

Spooling ECL spectroscopy is a method first developed by the Ding group that allows us to track the light emission process by obtaining individual spectrum at timed intervals.<sup>25</sup> Figure 2-5A indicates the spooling ECL spectra of the SSECL / BPO system obtained by scanning one cycle between 0.0 to -2.0 V at 0.1 V/s with one spectrum obtained every 0.25 s. The corresponding overlays of the individual spectra in the two scan directions shown in the inset highlight that all peaks center at  $\lambda_{\text{max}} = 630$  nm. As the emission wavelength remains unchanged throughout the ECL process, it is likely that a single excited state species is responsible for the light emission observed. The evolution and devolution of ECL generated from the SSECL / BPO system is consistent with the ECL-voltage curve utilizing a PMT as the detector (Figure 2-4A).



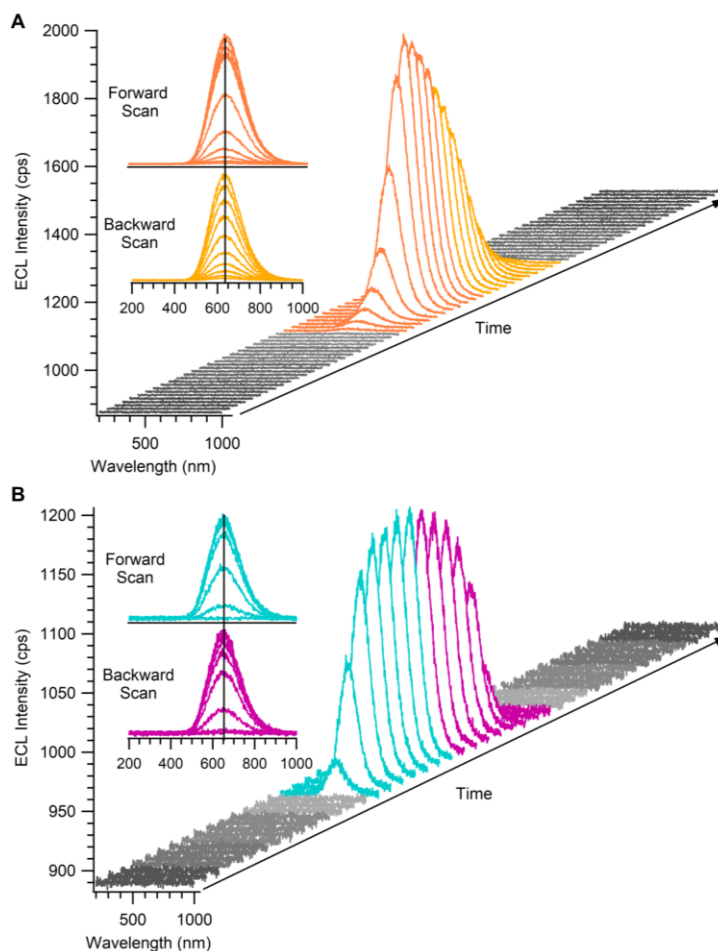


**Figure 2-5.** (A) Spooling ECL spectra of the SSECL / BPO coreactant system obtained by scanning from 0 to -2.0 V at 0.1 V/s with one spectrum taken every 0.25 s, inset shows an overlay of the individual spectra all centering at one wavelength,  $\lambda_{\text{max}} = 630$  nm. (B) Spooling ECL spectra of the homogenous DBC / BPO coreactant system obtained by scanning from 0 to -2.2 V at 0.1 V/s with one spectrum taken every 1 s. Inset indicates an overlay of the individual spectra all centering at one wavelength,  $\lambda_{\text{max}} = 650$  nm.

Similarly, the spooling ECL spectra of the homogenous DBC / BPO system were obtained by scanning one cycle between 0 to -2.2 V at 0.1 V/s with one spectrum taken every 1 s. The inset depicts the overlays of the individual spectra taken through the ECL process in two scan directions, and no change in the emission wavelength is observed. As a result, this reveals one excited state species. Furthermore, all peaks center at  $\lambda_{\text{max}} = 650$  nm. This emission wavelength closely matches the solution PL (black trace in Figure 2-

1A) and the SSECL / BPO (black trace in Figure 2-3). The 20 nm redshift difference in this homogenous coreactant system is attributed to the inner-filter effect. ECL of excimers composed of dimers and trimeric species often results in a red shifted emission up to 100 nm. Therefore, it is not likely that the observed redshift is a result of the excimers. The similar onset potential of ECL emission observed compared to the SSECL / BPO system (Figure 2-4A blue trace and B orange trace), provides further evidence that the electrochemical reduction of DBC initiates the ECL process.

Outlined in the bottom inset of Figure 2-3, the mechanism is shown for the BPO coreactant system. BPO is reduced to  $\text{BPO}^{\bullet-}$  upon scanning towards the cathodic region, leading to a consequent cleavage generating the  $\text{C}_6\text{H}_5\text{CO}_2^{\bullet}$  and  $\text{C}_6\text{H}_5\text{CO}_2^-$  species. At a further negative potential, the production and subsequent migration of  $\text{DBC}^{\bullet-}$  toward the solid/solution interface of the film occurs. The  $\text{DBC}^{\bullet-}$  reacts with the benzoate radical species already present in solution. It follows that the highly oxidizing species  $\text{C}_6\text{H}_5\text{CO}_2^{\bullet}$ , can extract an electron from the HOMO of  $\text{DBC}^{\bullet-}$  to generate the excited state species  $\text{DBC}^*$  ( $\lambda_{\text{ECL}} = 630 \text{ nm}$ ). The mechanism of the solution ECL / BPO system is similar to the one outlined in the bottom inset of Figure 2-3. All reactions occur in the vicinity of the electrode.

As demonstrated by the close resemblance of the SSECL / BPO emission to the solution PL, we attribute the strong luminescence enhancement primarily to the coreactant while likely, a secondary contribution from RIR. The ECL processes in the coreactant system occurs predominantly at the solid-solution interface, between the single molecular DBC layer of the crystalline film and BPO derivatives. At this interface, the DBC species are not well confined in the crystal lattice, therefore it is reasonable that CIE effects are not as pronounced in the SSECL / BPO systems. The increased concentration of DBC species within the film relative to the solution system may likely play a role in observing some emission enhancement, a natural and ubiquitous encounter when investigating ECL in the solid state. However, it is not inconceivable that RIR is still a key factor in the ECL enhancement observed with BPO. The similar increase in  $\Phi_{\text{ECL}}$  (5 times increase between the crystalline film and solution DBC) to that found in the absolute PL quantum yield

(nearly 4 times) further substantiates this claim. Moreover, the increase in ECL efficiency reiterates the high performing nature of the DBC as a solid-state emitter.

Therefore, as there is a push towards bright and low-cost luminophores, solid-state emitters that resist quenching are still lucrative. Here we have shown that crystallization induced emission/enhancements is a worthwhile path to achieve this goal. We hope this work provides a new perspective for tetracoordinate boron complexes and their use as a solid-state organic luminophore. The accurate ascribing of the ECL mechanisms was allowed for by testing multiple ECL systems while maintaining a focus on spectroscopy. As a growing number of studies probe SSECL, our future work aims to explore and address the interactions between coreactant and luminophore at the solid/solution interface. We seek to increase the RIR contribution towards ECL in the coreactant system while focusing on further developing the connection between CIE exhibiting complexes and their applications in ECL. The establishment of CIBS-ECL is a very promising start as we strengthen the concept of CIE while simultaneously demonstrating the diversity of ECL as a light emitting technique.

## 2.5 Experimental

The UV-visible absorbance spectra were obtained on a Varian Cary – 50 spectrophotometer. Photoluminescence experiments were performed on a Fluorolog instrument (QM-7/2005, Photon Technology International) with an excitation slit width of 0.25 au and an emission slit width of 0.1 au.

An electrochemical cell was utilized for cyclic voltammetry and subsequent ECL studies. The electrochemical cell consisted of a glass tube with a flat Pyrex window at the bottom to allow for the detection of ECL. The DBC was dissolved in a solution consisting of 0.1 M tetrabutylammonium hexafluorophosphate (TBAPF<sub>6</sub>, Sigma Aldrich) as the supporting electrolyte in 3 mL anhydrous acetonitrile. The electrochemical cell consisted of a three-electrode system which includes a modified glassy carbon working electrode, and two coiled Pt wires which served as the counter and reference electrode, respectively. The cell was assembled in an inert Ar atmosphere.

All cyclic voltammetry and ECL experiments were conducted on a CHI 610A electrochemical workstation (CH Instruments, Austin, TX). A photomultiplier tube (PMT, R928, Hamamatsu, Japan) held at a -750 V with a high voltage power supply was used to detect the ECL generated from the electrochemical cell. The photocurrent was measured and transformed to a voltage signal using a picoammeter/voltage source (Keithley 6487, Cleveland, OH). The potential, current and photocurrent signals obtained were recorded through a LabVIEW program (National Instruments). All ECL spectra were captured using an Andor DV429-BC CCD camera cooled to -65 °C.

## 2.6 References

1. Loudet, A.; Burgess, K., BODIPY Dyes and Their Derivatives: Syntheses and Spectroscopic Properties. *Chem. Rev.* **2007**, *107* (11), 4891-4932.
2. Li, D.; Zhang, H. Y.; Wang, Y., Four-coordinate Organoboron Compounds for Organic Light-emitting Diodes (OLEDs). *Chem. Soc. Rev.* **2013**, *42* (21), 8416-8433.
3. Liu, Z.; Jiang, Z.; Yan, M.; Wang, X., Recent Progress of BODIPY Dyes With Aggregation-Induced Emission. *Front. Chem.* **2019**, *7*, 712.
4. Hesari, M.; Lu, J. S.; Wang, S. N.; Ding, Z. F., Efficient Electrochemiluminescence of a Boron-dipyrromethene (BODIPY) Dye. *Chem. Commun.* **2015**, *51* (6), 1081-1084.
5. Rao, Y. L.; Wang, S. N., Four-Coordinate Organoboron Compounds with a pi-Conjugated Chelate Ligand for Optoelectronic Applications. *Inorg. Chem.* **2011**, *50* (24), 12263-12274.
6. An, B. K.; Kwon, S. K.; Jung, S. D.; Park, S. Y., Enhanced Emission and its Switching in Fluorescent Organic Nanoparticles. *J. Am. Chem. Soc.* **2002**, *124* (48), 14410-14415.
7. Zhao, Z.; Zhang, H.; Lam, J. W. Y.; Tang, B. Z., Aggregation-Induced Emission: New Vistas at the Aggregate Level. *Angew. Chem. Int. Ed.* **2020**, *59* (25), 9888-9907.
8. Luo, J. D.; Xie, Z. L.; Lam, J. W. Y.; Cheng, L.; Chen, H. Y.; Qiu, C. F.; Kwok, H. S.; Zhan, X. W.; Liu, Y. Q.; Zhu, D. B.; Tang, B. Z., Aggregation-induced Emission of 1-methyl-1,2,3,4,5-pentaphenylsilole. *Chem. Commun.* **2001**, (18), 1740-1741.
9. Leung, N. L. C.; Xie, N.; Yuan, W. Z.; Liu, Y.; Wu, Q. Y.; Peng, Q.; Miao, Q.; Lam, J. W. Y.; Tang, B. Z., Restriction of Intramolecular Motions: The General

- Mechanism behind Aggregation-Induced Emission. *Chem. Eur. J.* **2014**, *20* (47), 15349-15353.
10. Hong, Y. N.; Lam, J. W. Y.; Tang, B. Z., Aggregation-induced Emission: Phenomenon, Mechanism and Applications. *Chem. Commun.* **2009**, (29), 4332-4353.
  11. Dong, Y. Q.; Lam, J. W. Y.; Qin, A. J.; Li, Z.; Sun, J. Z.; Sung, H. H. Y.; Williams, I. D.; Tang, B. Z., Switching the Light Emission of (4-biphenyl)phenyldibenzofulvene by Morphological Modulation: Crystallization-induced Emission Enhancement. *Chem. Commun.* **2007**, (1), 40-42.
  12. Gong, Y. Y.; Zhao, L. F.; Peng, Q.; Fan, D.; Yuan, W. Z.; Zhang, Y. M.; Tang, B. Z., Crystallization-induced Dual Emission from Metal- and Heavy Atom-free aromatic acids and esters. *Chem. Sci.* **2015**, *6* (8), 4438-4444.
  13. Yang, S.; Yin, P. A.; Li, L.; Peng, Q.; Gu, X.; Gao, G.; You, J.; Tang, B. Z., Crystallization-Induced Reversal from Dark to Bright Excited States for Construction of Solid-Emission-Tunable Squaraines. *Angew. Chem. Int. Ed.* **2019**, DOI: 10.1002/anie.201914437.
  14. Bard, A. J., In *Electrogenerated Chemiluminescence*, 1 ed.; Bard, A. J., Ed. Marcel Dekker, Inc.: New York, NY 10016, U.S.A., 2004; p 533.
  15. Hesari, M.; Ding, Z., Review—Electrogenerated Chemiluminescence: Light Years Ahead. *J. Electrochem. Soc.* **2016**, *163* (4), H3116-H3131.
  16. Zhao, T.; Zhou, Q.; Lv, Y.; Han, D.; Wu, K.; Zhao, L.; Shen, Y.; Liu, S.; Zhang, Y., Ultrafast Condensation of Carbon Nitride on Electrodes with Exceptional Boosted Photocurrent and Electrochemiluminescence. *Angew. Chem. Int. Ed.* **2020**, *59* (3), 1139-1143.
  17. Wang, Y.; Jin, R.; Sojic, N.; Jiang, D.; Chen, H.-Y., Intracellular Wireless Analysis of Single Cells by Bipolar Electrochemiluminescence Confined in a Nanopipette. *Angew. Chem. Int. Ed.* **2020**, Ahead of Print.

18. Guo, W.; Ding, H.; Gu, C.; Liu, Y.; Jiang, X.; Su, B.; Shao, Y., Potential-Resolved Multicolor Electrochemiluminescence for Multiplex Immunoassay in a Single Sample. *J. Am. Chem. Soc.* **2018**, *140* (46), 15904-15915.
19. Guo, W.; Ding, H.; Zhou, P.; Wang, Y.; Su, B., Electrochemiluminescence Waveguide in Single Crystalline Molecular Wires. *Angew. Chem. Int. Ed.* **2020**, *59* (17), 6745-6749.
20. Nepomnyashchii, A. B.; Bard, A. J., Electrochemistry and Electrogenated Chemiluminescence of BODIPY Dyes. *Acc. Chem. Res.* **2012**, *45* (11), 1844-1853.
21. Booker, C.; Wang, X.; Haroun, S.; Zhou, J.; Jennings, M.; Pagenkopf, B. L.; Ding, Z., Tuning of Electrogenated Silole Chemiluminescence. *Angew. Chem. Int. Ed.* **2008**, *47* (40), 7731-7735.
22. Miao, W. J.; Choi, J. P.; Bard, A. J., Electrogenated Chemiluminescence 69: The Tris(2,2'-bipyridine)Ruthenium(II), (Ru(bpy)<sub>3</sub><sup>2+</sup>)/Tri-n-propylamine (TPrA) System Revisited - A New Route Involving TPrA<sup>•+</sup> Cation Radicals. *J. Am. Chem. Soc.* **2002**, *124* (48), 14478-14485.
23. Hesari, M.; Swanick, K. N.; Lu, J. S.; Whyte, R.; Wang, S. N.; Ding, Z. F., Highly Efficient Dual-Color Electrochemiluminescence from BODIPY-Capped PbS Nanocrystals. *J. Am. Chem. Soc.* **2015**, *137* (35), 11266-11269.
24. Ding, Z. F.; Quinn, B. M.; Haram, S. K.; Pell, L. E.; Korgel, B. A.; Bard, A. J., Electrochemistry and Electrogenated Chemiluminescence from Silicon Nanocrystal Quantum Dots. *Science* **2002**, *296* (5571), 1293-1297.
25. Swanick, K. N.; Hesari, M.; Workentin, M. S.; Ding, Z. F., Interrogating Near-Infrared Electrogenated Chemiluminescence of Au<sub>25</sub>(SC<sub>2</sub>H<sub>4</sub>Ph)<sub>18</sub><sup>+</sup> Clusters. *J. Am. Chem. Soc.* **2012**, *134* (37), 15205-15208.
26. Richter, M. M., Electrochemiluminescence (ECL). *Chem. Rev.* **2004**, *104* (6), 3003-3036.

27. Downey, T. M.; Nieman, T. A., Chemiluminescence Detection Using Regenerable Tris(2,2'-Bipyridyl)Ruthenium(II) Immobilized in Nafion. *Anal. Chem.* **1992**, *64* (3), 261-268.
28. Pei, Q. B.; Yu, G.; Zhang, C.; Yang, Y.; Heeger, A. J., Polymer Light-Emitting Electrochemical-Cells. *Science* **1995**, *269* (5227), 1086-1088.
29. Swanick, K. N.; Ladouceur, S.; Zysman-Colman, E.; Ding, Z. F., Self-Enhanced Electrochemiluminescence of an Iridium(III) Complex: Mechanistic Insight. *Angew. Chem. Int. Ed.* **2012**, *51* (44), 11079-11082.
30. Kim, J. I.; Shin, I. S.; Kim, H.; Lee, J. K., Efficient Electrogenerated Chemiluminescence from Cyclometalated Iridium(III) Complexes. *J. Am. Chem. Soc.* **2005**, *127* (6), 1614-1615.
31. Carrara, S.; Aliprandi, A.; Hogan, C. F.; De Cola, L., Aggregation-Induced Electrochemiluminescence of Platinum(II) Complexes. *J. Am. Chem. Soc.* **2017**, *139* (41), 14605-14610.
32. Gao, T. B.; Zhang, J. J.; Yan, R. Q.; Cao, D. K.; Jiang, D.; Ye, D., Aggregation-Induced Electrochemiluminescence from a Cyclometalated Iridium(III) Complex. *Inorg. Chem.* **2018**, *57* (8), 4310-4316.
33. Saremi, M.; Amini, A.; Heydari, H., An Aptasensor for Troponin I Based on the Aggregation-induced Electrochemiluminescence of Nanoparticles Prepared from a Cyclometalated Iridium(III) Complex and Poly(4-vinylpyridine-co-styrene) Deposited on Nitrogen-doped Graphene. *Microchim. Acta* **2019**, *186* (4).
34. Wei, X.; Zhu, M. J.; Cheng, Z.; Lee, M.; Yan, H.; Lu, C. S.; Xu, J. J., Aggregation-Induced Electrochemiluminescence of Carboranyl Carbazoles in Aqueous Media. *Angew. Chem. Int. Ed.* **2019**, *58* (10), 3162-3166.
35. Han, Z. G.; Yang, Z. F.; Sun, H. S.; Xu, Y. L.; Ma, X. F.; Shan, D. L.; Chen, J.; Huo, S. H.; Zhang, Z.; Du, P. Y.; Lu, X. Q., Electrochemiluminescence Platforms



Based on Small Water-Insoluble Organic Molecules for Ultrasensitive Aqueous-Phase Detection. *Angew. Chem. Int. Ed.* **2019**, *58* (18), 5915-5919.

36. Saikin, S. K.; Einfeld, A.; Valleau, S.; Aspuru-Guzik, A., Photonics Meets Excitonics: Natural and Artificial Molecular Aggregates. *Nanophotonics* **2013**, *2* (1), 21-38.
37. Wu, Q. Y.; Zhang, T.; Peng, Q.; Wang, D.; Shuai, Z. G., Aggregation Induced Blue-shifted Emission - the Molecular Picture from a QM/MM Study. *Phys. Chem. Chem. Phys.* **2014**, *16* (12), 5545-5552.
38. Yamauchi, M.; Yokoyama, K.; Aratani, N.; Yamada, H.; Masuo, S., Crystallization-Induced Emission of Azobenzene Derivatives. *Angew. Chem. Int. Ed.* **2019**, *58* (40), 14173-14178.
39. Cao, W. D.; Zhang, X. H.; Bard, A. J., Electrogenerated Chemiluminescence. 75. Electrochemistry and ECL of 9,10-bis(2-naphthyl)anthracene. *J. Electroanal. Chem.* **2004**, *566* (2), 409-413.

## Chapter 3

### 3 Discovering the Link between the Electrochemiluminescence and Energy Transfers/Surface States of Mn-Doped CsPbCl<sub>3</sub> Perovskites

#### 3.1 Introduction

Perovskite nanomaterials have been garnering huge interest as of late owing to their diverse opto-electronic properties, allowing for applications in solar cell energy conversion and light emitting devices.<sup>1-3</sup> One subset is the all-inorganic cesium lead halide (CsPbX<sub>3</sub>, X = Cl, Br, I) perovskite semiconducting nanocrystals (NCs) which are rapidly developing materials as they boast high photoluminescence (PL) efficiencies (near unity), facile low cost one-pot synthetic methods, narrow and tunable emission peaks, and possess a tailorable band gap.<sup>4-7</sup> Metal doping can lead to great benefits in semiconducting nanomaterials.<sup>8-9</sup> The relatively large space within and between PbX<sub>6</sub><sup>4-</sup> octahedra allows for facile ion doping both during and post synthesis, inviting new emissive pathways and properties.<sup>7</sup> Previous studies on doped CsPbCl<sub>3</sub> NCs have documented that the presence of a dopant promotes short-ranged lattice order and a selective group of metals introduce a secondary emissive channel in addition to the pristine perovskite emission.<sup>4, 10-11</sup> Unique to Mn<sup>2+</sup> doping which replaces a fraction of the Pb atoms in the CsPbCl<sub>3</sub> lattice, results in the formation CsPb<sub>1-x</sub>Mn<sub>x</sub>Cl<sub>3</sub>, is the ability to observe a characteristic orange/red emission that stems from the sensitized <sup>4</sup>T<sub>1g</sub> → <sup>6</sup>A<sub>1g</sub> d-d relaxation.<sup>12</sup> This new emissive channel is accessed through the host-dopant dynamics as in doped semiconductor nanocrystals.<sup>13</sup>

Electrochemiluminescence (ECL) is a phenomenon during which light is generated by electrochemical reactions instead of an external light source.<sup>14-15</sup> ECL has been widely employed in antigen-detecting bioanalytical assays.<sup>16</sup> However, as traditional high-cost ruthenium-based complexes are often employed, ECL studies of quantum dots (QDs) have grown exponentially in hopes of identifying alternative efficient and low-cost luminophores.<sup>17-18</sup> Although the perovskite's candidacy in electroluminescence has since been studied in a few reports,<sup>19-20</sup> investigation on the ECL performance is still in its

infancy.<sup>21-23</sup> To date, no studies have probed the ECL of doped perovskites. Quite notably, a few ECL studies on all-inorganic perovskites have only explored the CsPbBr<sub>3</sub> variety, likely as preliminary studies have pointed towards their higher PL efficiencies relative to the CsPbCl<sub>3</sub> counterpart.<sup>24-30</sup> However, CsPbBr<sub>3</sub> encounters a dilemma due to the small bandgap of the NCs which significantly reduces the observed d-d relaxation in the host-dopant emission involving the Mn<sup>2+</sup> dopant.<sup>7</sup> This issue is circumvented by utilizing the CsPbCl<sub>3</sub> host perovskite which well encapsulates the Mn-dopant's bandgap within its own. Therefore, in hopes of gaining new insights into the host-dopant emission mechanism, we study the ECL characteristics of Mn-doped CsPbCl<sub>3</sub> quantum dots (MPQ) and CsPbCl<sub>3</sub> undoped quantum dots (UPQ).

One key point to note is that while metal complexes<sup>31-32</sup>, organic molecules<sup>33</sup> and metal clusters<sup>34</sup> often exhibit similar PL and ECL emission wavelengths, QDs often display surface state emissions that differs from their PL.<sup>18, 35-36</sup> It has long been associated that ECL often probes surface states while the PL frequently probes the core of the NCs.<sup>36-37</sup> However, the ramifications of surface state relaxation remain underdeveloped as few studies elaborate and discuss the possible sources that can impact surface state emission which is observed in the QDs.<sup>38</sup> Therefore, insights into the surface state emission are valuable and integral to future studies in understanding ECL of QDs.

In this work, we demonstrate for the first time, the host-dopant energy transfer mechanism as it pertains to ECL of perovskites. We compare both the UPQ and the MPQ's ECL performance in order to propose a fitting mechanism that captures the interesting spectral properties observed by both materials. Through the detailed comparison between the PL and ECL emission properties, we correlate the observed ECL features obtained through electrochemical and photoelectrochemical spectroscopy to the well documented PL host-dopant energy transfer mechanism.

## 3.2 Results

PL studies were first utilized to probe the emissive pattern of the UPQ and MPQ dispersed in hexanes, Figure 3-1. Following photoexcitation at  $\lambda_{\text{ex}} = 355$  nm, the UPQs (Figure 3-1A-blue trace) displayed a weak intensity emission at  $\lambda_{\text{max}} = 405$  nm.

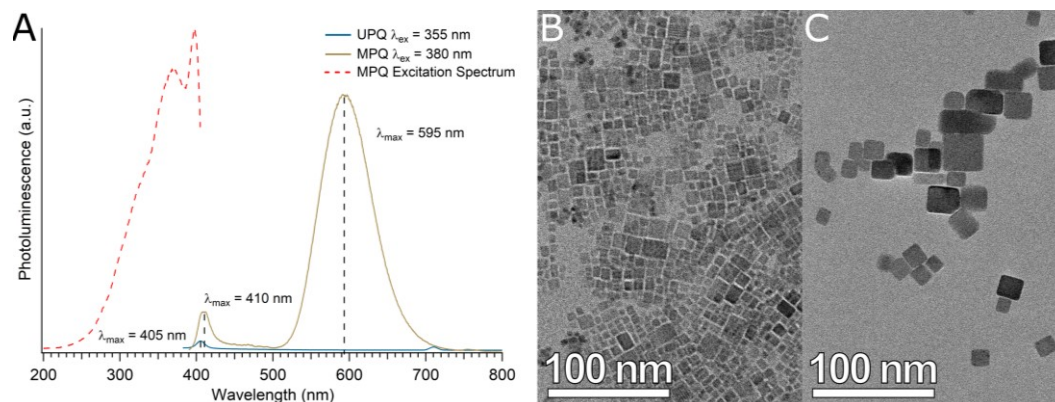


**Figure 3-1.** (A) PL spectra of the undoped  $\text{CsPbCl}_3$  perovskite (UPQ - blue trace), doped  $\text{Mn-CsPbCl}_3$  perovskite (brown trace) and the MPQ excitation spectrum (red trace). TEM images of (B) MPQ and (C) UPQ.

This emission peak agrees well with previously reported literature and is the result of the  $\text{CsPbCl}_3$  perovskite quantum dot core (band gap).<sup>39</sup> The subsequent PL emission of the MPQs ( $\lambda_{\text{ex}} = 380 \text{ nm}$ ) is shown in Figure 3-1A-brown trace, where two peaks are observed: a retention of the weak violet emission at  $\lambda_{\text{max}} = 410 \text{ nm}$  is attributed to the intrinsic  $\text{CsPbCl}_3$  lattice (host), while the broad orange emission found at  $\lambda_{\text{max}} = 595 \text{ nm}$  arises due to a small fraction of excitons that undergoes an energy transfer to the Mn dopant level within the perovskite (dopant). The absolute PL quantum yield ( $\Phi_{\text{PL}}$ ) was determined to be 20.9 % for the MPQ, a nearly two times increase was found compared to the 10.7 % obtained for the UPQ. A PL enhancement in the MPQ host emission is also observed relative to the UPQ. Defects in the perovskite lattice have been attributed to lower PL efficiencies in the UPQ. Most notably, chloride vacancies act as electron traps reducing the radiative emission.<sup>40</sup> However, upon doping with Mn, reduction of chloride vacancies has been well documented because of the simultaneously increased  $\text{Cl}^-$  concentration upon  $\text{MnCl}_2$  precursor introduction.<sup>41-42</sup> Figure 3-1B and 3-1C highlights the TEM images of the MPQ and UPQ, respectively, which indicate that a cubic structure was observed for both perovskite NCs. It is interesting to note that upon introduction of a Mn dopant, the NCs formed exhibit a smaller size relative to their undoped counterparts. This is likely due to the incorporation of Mn into the lattice which possesses a smaller radius relative to Pb. As

a result, crystal shrinking is observed. Furthermore, ICP-MS indicates that Mn concentration was achieved at 3.1 % within the doped CsPbCl<sub>3</sub> perovskite.

### 3.3 Electrochemistry and Electrochemiluminescence on the MPQ and UPQ

To gain an understanding of their electrochemical properties, cyclic voltammetry (CV) was performed on both UPQ and MPQ to determine their electrochemical profile. The CV and corresponding ECL-voltage curves for the MPQs are highlighted in Figure 3-2A.

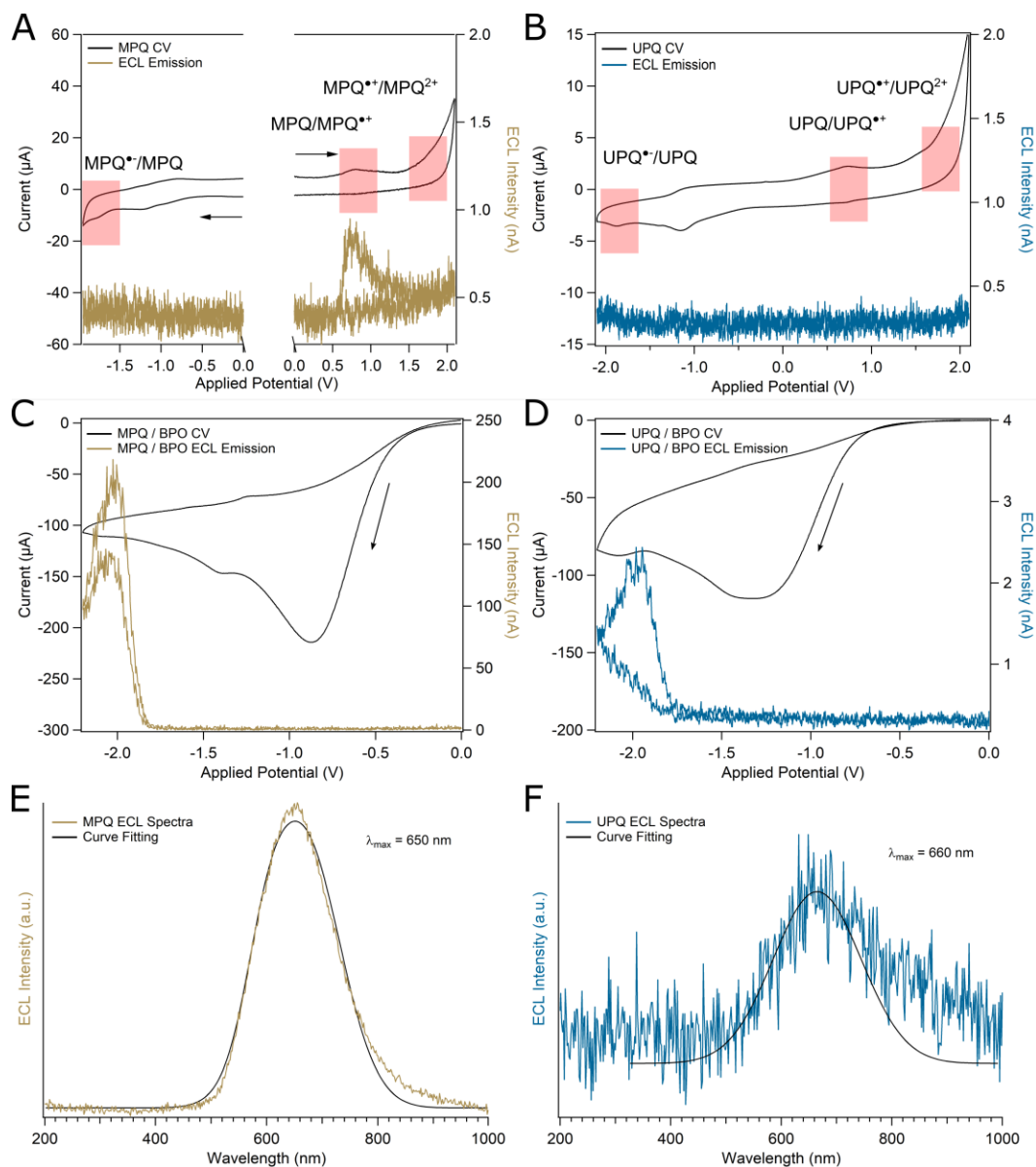


**Figure 3-2.** Cyclic voltammograms and corresponding ECL-voltage curves of GCEs modified with 280  $\mu\text{g}$  MPQ in 0.1 M TBAPF<sub>6</sub> ACN solution (A), 280  $\mu\text{g}$  UPQ in 0.1 M TBAPF<sub>6</sub> ACN solution (B), 280  $\mu\text{g}$  MPQ in 0.1 M TBAPF<sub>6</sub> ACN solution containing 5 mM BPO (C), and 280  $\mu\text{g}$  MPQ in 0.1 M TBAPF<sub>6</sub> ACN solution containing 5 mM BPO (D). The scan rate is 0.1 V/s. Accumulated ECL spectra obtained by pulsing between two potentials for 60 seconds and corresponding curve fitting obtained from MPQ / BPO (E) and UPQ / BPO (F) systems, respectively.

The quantum dots, unlike many metal complexes that have defined metal centers undergoing oxidation state changes, are semiconducting nanomaterials that often exhibit broad and less defined electrochemical features. As a result, we utilize the ECL-voltage curve alongside the cyclic voltammogram to confirm the presence of electrochemical oxidation/reduction. At the MPQ film electrode, two oxidation peaks are observed, at 0.77 V and 1.54 V, while one reduction peak is seen at -1.70 V (Figure 3-2A). These potentials correspond to  $\text{MPQ}/\text{MPQ}^{\bullet+}$ ,  $\text{MPQ}^{\bullet+}/\text{MPQ}^{2+}$ , and  $\text{MPQ}/\text{MPQ}^{\bullet-}$ , respectively. A peak at -1.27 V might be the adsorption of MPQ onto the GCE surface. Additionally, ECL-voltage curves provide information about the potential-dependent light emission that is triggered by the annihilation of electrogenerated radicals. By looking at the ECL voltage curve (brown trace, Figure 3-2A), we observe a pronounced ECL peak at +0.72 V and a gradual evolution and devolution in intensity till +1.64 V. The close agreement between the ECL-voltage curve and CV indicates that electrogenerated redox events instigate ECL via radical annihilation. It is interesting to note that ECL was only generated in the scan towards the anodic region.

Similarly, in the CV and ECL-voltage curves of UPQs (Figure 3-2B), two oxidation peaks are observed with the UPQs at 0.8 V ( $\text{UPQ}/\text{UPQ}^{\bullet+}$ ) and at 1.2 V ( $\text{UPQ}^{\bullet+}/\text{UPQ}^{2+}$ ) alongside one reduction event seen at -1.7 V ( $\text{UPQ}/\text{UPQ}^{\bullet-}$ ). Previously, Kamat, Janáky and coworkers investigated  $\text{CsPbBr}_3$  perovskite nanocrystals and report three electrochemical events at similar potentials to the UPQ (-1.4 V, +0.8 V and +1.5 V).<sup>24</sup> With bromide incorporation into the perovskite lattice being the distinguishing factor, their study provides a reasonable guideline to expect that  $\text{CsPbCl}_3$  should exhibit similar electrochemical features. Correspondingly, the UPQs display a similar electrochemical profile to the MPQs as Mn-doping should not significantly alter the host perovskite lattice. However, no ECL was generated. This is likely due to the stability of the UPQ radical species electrogenerated which are not enough for the observation of light emission during potential scanning. Therefore, it is evident that upon addition of a Mn dopant to the  $\text{CsPbCl}_3$  perovskite, ECL is observed in the annihilation pathway due to increased stability of the charged states relative to the undoped perovskite. The ECL efficiency ( $\Phi_{\text{ECL}}$ ), relative to the  $[\text{Ru}(\text{bpy})_3]^{2+}$  standard, of the MPQ in the annihilation pathway was determined to be 0.08 %. The low efficiency is quite understandable, as the perovskite is unstable at ambient preparation and

testing conditions. Chloride deficiencies and traps obtained through inevitable purification and washing of the oleyamine protecting ligand required for electrochemical testing would further compromise the structural integrity and lead to lower efficiencies.<sup>43</sup> Further elaboration on the ECL efficiency will be discussed later.

The addition of a coreactant often enhances the ECL observed by interacting with the electrogenerated radical species.<sup>33</sup> Based on the CV and ECL-voltage curves in Figure 3-2A that indicate the more stable radical anion species, benzoyl peroxide (BPO) was chosen as the coreactant. Upon the addition of 5 mM BPO, a 230 times increase in ECL intensity was observed for the MPQ, reaching 230 nA at a 0.1 V/s scan rate in Figure 3-2C relative to that of the annihilation pathway (1 nA in Figure 3-2A). As the potential is scanned negative, BPO reduction occurs at -0.865 V and consequently MPQ/MPQ<sup>•-</sup> reduction occurs at -1.70 V. The evolution of ECL is then observed at -1.78 V, matching well with the reduction potential of the MPQs, confirming that MPQ<sup>•-</sup> is required for the evolution of light. The high oxidation power of the benzoate radical and close reduction potential proximity to the generation of MPQ<sup>•-</sup> / UPQ<sup>•-</sup> enforce a strong ECL emission.<sup>44</sup> Similarly, in the presence of 5 mM BPO, ECL is observed for the UPQ although only reaching 2.3 nA at a 0.1 V/s scan rate (Figure 3-2D). First, BPO is reduced at -1.28 V (potential shift likely due to the presence of a less conductive film) and upon scanning further negative, UPQ/UPQ<sup>•-</sup> reduction occurs at -1.70 V. The ECL onset potential at -1.765 V (blue trace) matches well with the UPQ reduction potential and attributes the light emission to the existence of UPQ<sup>•-</sup> species. The presence of a Mn-dopant in the MPQs has led to a 100 times enhancement in the ECL intensity observed versus the undoped CsPbCl<sub>3</sub> quantum dot with a coreactant, signifying a high prospect for metal doping in nanomaterials. In such a case, we also wish to portray the ECL efficiency of MPQ relative to the UPQ as it speaks to the beneficial nature of Mn doping. The calculated relative ECL efficiency was found to be 20 times increased or 2000 %. Nonetheless, efficiency does not affect the interesting spectral properties that are observed from the MPQ and UPQ ECL emission.

As ECL was observed for both MPQ and UPQ with 5 mM BPO, an accumulated spectrum was taken for both systems by means of potential pulsing in order to shorten the



time for coreactant and quantum dot radicals to meet. The corresponding ECL spectrum for the MPQ / BPO system is shown in Figure 3-2E in which a broad peak with a peak wavelength of 650 nm is observed. Meanwhile, for the UPQ / BPO system, a peak with a  $\lambda_{\max} = 660$  nm was observed in the ECL spectrum (Figure 3-2F). This corresponds to a substantial 260 nm red shift in the ECL emission relative the excitonic PL of the UPQ (Figure 3-1B). Since strong ECL was obtained for the MPQ / BPO, spooling ECL spectroscopy (an in-situ testing method developed by the Ding group) was employed to further study the light emission.<sup>34</sup> Figure 3-3 exhibits the spooling ECL spectra obtained by scanning the potential window from 0 to -2.2 V and back to 0 V at a scan rate of 0.1 V/s with a spectrum taken every 1 s. This allows us to accurately observe any changes in the ECL through the entire potential scan.

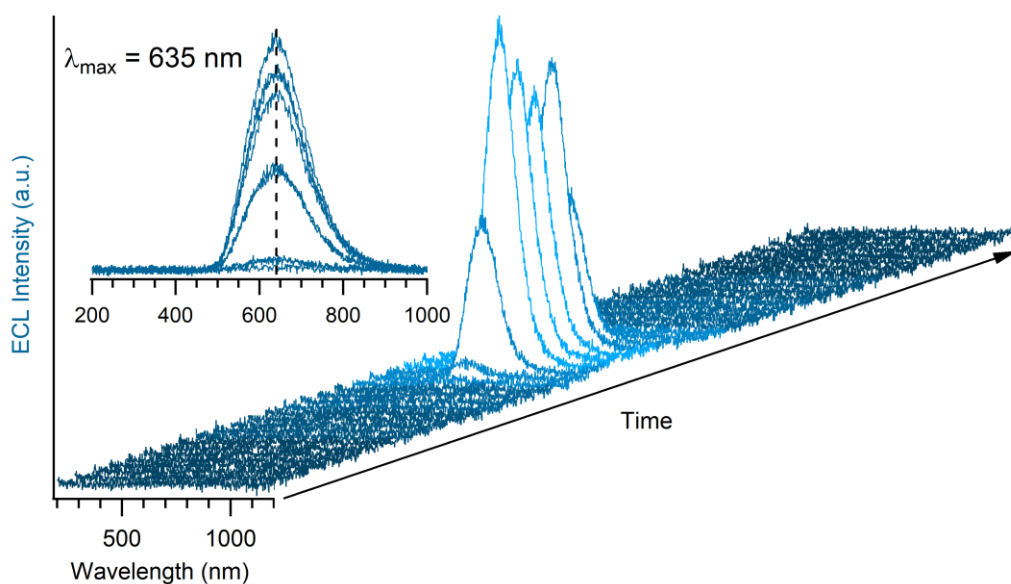


**Figure 3-3.** Spooling ECL spectra of the MPQ / BPO coreactant system obtained by scanning from 0 to -2.2 V and back to 0 V at 0.1 V/s with one spectrum taken every 1 s. Inset shows an overlay of the individual spectra all centering at one wavelength  $\lambda_{\max} = 635$  nm.

The inset depicts the overlay of all the spectra taken throughout the ECL evolution and devolution. All peaks center at  $\lambda_{\max} = 635$  nm and no changes in emission were observed. Seemingly, as the  $\lambda_{\max}$  detected via ECL bears no resemblance to the PL of

either UPQ or MPQ (Figure 3-1B), the default explanation would be the relaxation of excited state species to surface states which would often produce red shifted emission. However, through curve fitting, we further examined the spooling ECL spectra of the MPQ / BPO system.

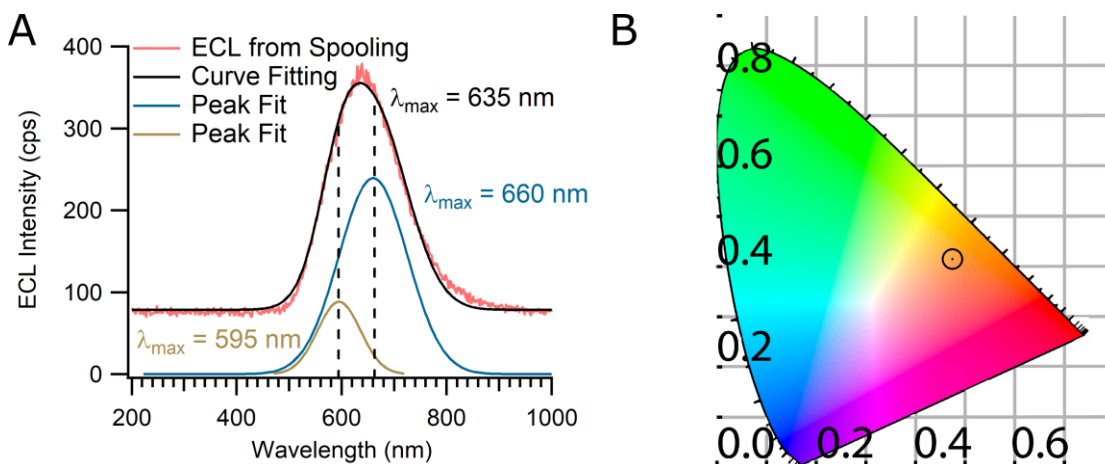
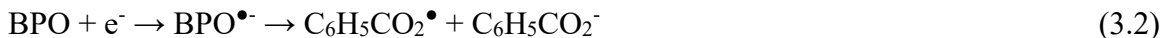


**Figure 3-4.** (A) One ECL spectrum extracted from spooling ECL spectroscopy (Figure 3-3 – scan 21 taken at -2.1 V on the scan towards the cathodic region - red trace) with the corresponding curve fit (black trace) and peak fit (brown and blue trace) for MPQ. (B) *Commission internationale de l'éclairage* chromaticity diagram of the ECL spectrum in (A).

The highest intensity spectrum was first extracted from the spooling ECL spectra (scan 21 at -2.1 V of Figure 3-3). By fitting a  $\lambda_{\max} = 595$  nm peak to the extracted spooling ECL spectrum, a second peak at  $\lambda_{\max} = 660$  nm arises (Figure 3-4A). Very interestingly, this peak,  $\lambda_{\max} = 660$  nm, matches well to the ECL emission obtained by pulsing the potential window of the UPQ / BPO system (Figure 3-2F). In the absence of a secondary emissive channel, the UPQs have no means of undergoing energy transfer, it is reasonable to assign the 660 nm ECL emission as derived from excited surface state. A Commission internationale de l'éclairage chromaticity diagram indicates that a deep orange color was obtained from the spooling ECL spectrum (Figure 3-4B). The 260 nm red shift observed for the UPQ ECL relative to the PL further alludes to this surface state relaxation. The straightforward nature of the UPQ allows us to propose the following ECL mechanism for the coreactant pathway. Upon scanning towards the cathodic region, UPQ is reduced to

form UPQ<sup>•-</sup> (Eq. 3.1). At a further negative potential, BPO is reduced and subsequently cleaves to form the benzoate radical, C<sub>6</sub>H<sub>5</sub>CO<sub>2</sub><sup>•</sup>, (Eq. 3.2). The benzoate radical can then proceed to oxidize the UPQ<sup>•-</sup> to form the excited state species, UPQ<sup>\*</sup>, which then relaxes to emit light at 660 nm (Eq. 3.3 and 3.4).



### 3.4 Discussion

Before addressing the ECL of the MPQ coreactant pathway, we must first ascertain the mechanism for the MPQ in the annihilation route. Photoexcitation of the perovskite host in the MPQ is critical in observing the consequential emission of the Mn dopant. Therefore, there is an expectation that electrochemical excitation must also impart (or maintain available) an equivalent magnitude of energy. An approximation can be made for the energy required for singlet transition ( $E_s$ ) based on the conversion from the wavelength of the perovskite host emission ( $\lambda_{\text{max}} = 410 \text{ nm}$ ) utilizing Eq. 3.5.<sup>45</sup> A 3.02 eV requirement is necessary from electrochemical excitation.

$$E_s = \frac{1239.81}{\lambda \text{ (in nm)}} \quad (3.5)$$

In order to generate the excited state, the enthalpy of ECL generation reactions determined from the peak potentials of the redox waves should be greater than that of the excited states determined from the emission peak wavelength:

$$E_p(R'/R'^+) - E_p(R/R^-) - 0.16 \text{ (eV)} \geq -\Delta H^\circ \quad (3.6)$$

where  $E_p(R'/R'^+)$  and  $E_p(R/R^-)$  can be calculated from the oxidation and reduction peak potentials, respectively, obtained from CVs;  $-\Delta H^\circ$  represents the enthalpy or the available energy of the ECL system.<sup>44, 46</sup> For the annihilation reactions, 2.34 eV is obtained

which is inferior to 3.02 eV required for host excitation and consequent energy transfer. As  $-\Delta H^{\circ}_{\text{annihilation}}$  is smaller than  $E_s$ , it is believed that generating the  $\text{MPQ}^*$  occurs via triplet-triplet annihilation (TTA). This has commonly been referred to as the energy insufficient pathway and is highlighted in Figure 3-5A.

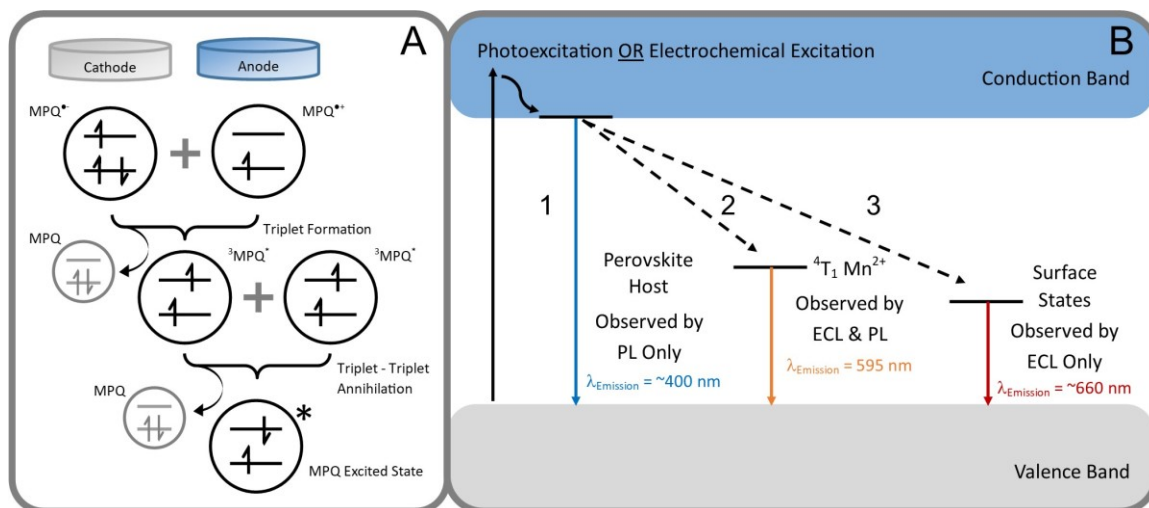


**Figure 3-5.** (A) The triplet-triplet annihilation pathway mechanism is outlined for the MPQ. (B) A diagram of the three emissive pathways (1. host, 2. dopant and 3. surface state) that are observed through PL and ECL of the MPQ.

As we first scan towards the cathodic region,  $\text{MPQ}^{\bullet-}$  is generated and its good stability allows for the species to remain present in the film. As the potential is then biased positively,  $\text{MPQ}^{\bullet+}$  is generated. The two electrogenerated species meet in the nanocrystalline film and an electron transfer occurs to produce one ground state (MPQ) and one triplet state species ( $^3\text{MPQ}^{\bullet}$ ). Two triplet state species can then meet and undergo an electron transfer reaction (TTA) to yield a singlet excited state species ( $\text{MPQ}^*$ ), which can then relax to emit light. Although ECL was not sufficient to obtain a spectrum, we would like to discuss the probable origins of light emission in the annihilation pathway.

It is easy to attribute the observed ECL as surface state emissions, however, alternatives must be considered before establishing the most likely route. We must consider the possibility of directly probing the Mn d-d transition through electrochemical excitation. This is substantiated as the  $-\Delta H^{\circ}_{\text{annihilation}} = 2.34 \text{ eV}$  is sufficient for a 595 nm singlet excited

state formation. However, it is widely established that photoexcitation of the perovskite bandgap is necessary for the sensitization of the Mn d-d transition. This concept is further strengthened by the intensity of ECL observed in the MPQ annihilation pathway. The low intensity ECL signifies that likely an energy insufficient pathway is occurring. If electrochemical excitation of the MPQ directly probed the Mn d-d transition, an energy sufficient singlet state formation would likely lead to a higher observed ECL intensity. Therefore, the spectral evidence leads us to hypothesize that the MPQ annihilation pathway leads to surface state relaxation through TTA.

The MPQ coreactant pathway requires the formation of the excited state species,  $\text{MPQ}^*$ , which occurs in a similar manner to the mechanism for  $\text{UPQ}^*$  (Eq. 3.1-3.3). However, it is the relaxation of the  $\text{MPQ}^*$  that we wish to elaborate further as we propose a dual emissive pathway. For the coreactant reactions to generate the excited state, they rely on both the reduction peak potential of the  $\text{MPQ} / \text{MPQ}^{\bullet-}$  and the contribution of the benzoate radical  $\text{C}_6\text{H}_5\text{CO}_2^{\bullet}$ . This radical possesses a strong oxidation power, which warrants the use of BPO as a coreactant. Early studies by Chandross investigated the oxidation power of the benzoate radical pertaining to its contributions towards ECL emission observed in the coreactant pathway.<sup>47-48</sup> Upon BPO reduction and consequent cleavage, the benzoate radical is generated with an oxidation power  $E_{\text{benzoate}^{\bullet}} = 1.5 \text{ V}$ .<sup>44, 49-50</sup> The calculated enthalpy for the coreactant reaction is 3.04 eV. It must be noted that although 3.04 eV is sufficient for MPQ host excitation, this does not provide a large excess of energy ( $\sim 0.02 \text{ eV}$ ). As a result, when comparing between the two pathways for excited state species relaxation, surface state relaxation would be preferential as the energy required for host excitation and consequent energy transfer is marginally met. Therefore, this is one likely reason why low contributions from the Mn emission are observed in Figure 3-4A. A diagram is shown in Figure 3-5B that summarizes the three emissive channels observed by either PL or ECL. In PL, both host and dopant emission are observed (blue and orange arrows). Yet, upon electrochemical excitation, host emission is no longer detected but rather a surface state emission arises. Evidently, upon comparing the peaks obtained through curve fitting (Figure 3-4A) to the UPQ surface state emission (Figure 3-2F), the similar  $\lambda_{\text{max}}$  and sufficient energy for excited singlet state formation persuades us

to believe that two emissive channels are similarly occurring in ECL, paths 2 and 3 in Figure 3-5B.

Furthermore, three distinct points observed in the experimental data strongly persuade us to believe that a dual emission is likely occurring in the ECL of MPQ.

- (1) As shown in Figure 3-2F, the UPQ / BPO spectrum allows us to assign the UPQ's emission as one due to surface states. This is due to the prominent 260 nm red shift observed from the PL of the UPQ (Figure 3-1B) relative to the ECL. The first report on the ECL of Si quantum dots highlights that ECL emission to surface states can produce quite a red shifted emission ( $\lambda_{\text{max-ECL}} = 640 \text{ nm}$ ,  $\sim 220 \text{ nm}$  red shifted from the  $\lambda_{\text{max-PL}} = 420 \text{ nm}$ ).<sup>37</sup> Furthermore, this aids us in identifying the MPQs surface state relaxation contribution (blue trace in Figure 3-4A). CsPbCl<sub>3</sub> and Mn-doped CsPbCl<sub>3</sub> nanocrystals can be synthesized to have matching absorption spectra and similar size.<sup>40</sup> However, potential surface defects of the perovskite nanocrystals would heavily alter the observed ECL emission wavelength. We assume that dopant distribution is random in the nanocrystal however it is noted that any Mn present near the surface is likely fully coordinated by Cl<sup>-</sup> as there is an absence in heterogeneous dynamics from the Mn PL.<sup>40</sup> Therefore, reasonable approximations can be concluded that UPQ / MPQ surface state emission should be in close agreement. As a result, the  $\sim 660 \text{ nm}$  peak that arises from fitting one at 595 nm in Figure 3-4A of the MPQ can be identified as one stemming from relaxation to surface state path 3 in Figure 3-5B.
- (2) As previously highlighted, the contribution from the 595 nm Mn emission in the ECL is low in proportion to the surface state contribution (660 nm) as shown in Figure 3-4. One reason is due to the marginal surplus in energy from the coreactant reactions. However, it is normal that this feature is observed if a dual emission is indeed occurring. ECL is a surface state sensitive technique since quantum dots undergo electrochemical reactions at surface active spots<sup>36</sup> and as

a result, the 660 nm emission would be favored. Likely, for dual emission ECL, a cooccurrence between these two competitive pathways must ensue.

- (3) Finally, we must address the surface state emission enhancement observed in the MPQ relative to the UPQ which can be attributed to structural properties. Many cases of small quantity Mn impurity doping in CsPbCl<sub>3</sub> perovskites have shown a PL exciton emission enhancement relative to the undoped version.<sup>40-42</sup> This exciton emission enhancement occurs unless the host crystallinity is heavily impacted by the integration of large quantities of Mn, as its atomic size is smaller than Pb, leading to the reduction in PL.<sup>51</sup> Intrinsically the CsPbCl<sub>3</sub> perovskite possesses Cl vacancies that act as electron traps, leading to non-radiative energy loss. Nevertheless, lowered quantities of these vacancies allowing for higher PL exciton performance due to the decrease in structural defects has been attributed to Mn doping.<sup>52</sup> Therefore, it is understandable that the MPQ's ECL emission to surface states also exhibits enhancement due to the reduction of defects that is more prevalent in the UPQ.

In summary, physical insight into the drastic difference in emissive states of Mn-doped perovskite quantum dots has been obtained. Subtleties in the spectral data have allowed for the elucidation and assigning of a dual-emissive ECL pathway of the MPQ through energy transfers and surface states. The ability to realize PL effects in ECL not only speaks to the versatility of all-inorganic perovskites but demonstrates the strength of ECL as a tool to effectively study their emissive capabilities. This brings forth a second breath to ECL studies as new doped nanomaterials are constantly emerging with interesting optical and electronic properties. It is our hope that this work lays a foundation for future ECL studies in the vast field of quantum dot chemistry. Although surface state emission has remained a staple to the field of quantum dot ECL, we believe that it is not out of reach to lower surface state contributions and increase the radiative processes of core relaxation that are primarily probed by PL. Furthermore, we hope that this study provides insight towards the engineering and applications of new light emitting semiconducting nanomaterials.

### 3.5 Experimental

The UV-visible absorbance spectra were obtained on a Varian Cary – 50 spectrophotometer. Photoluminescence experiments were performed on a Fluorolog instrument (QM-7/2005, Photon Technology International) with an excitation slit width of 0.25 au and an emission slit width of 0.1 au.

An electrochemical cell was utilized for cyclic voltammetry and subsequent ECL studies. The electrochemical cell consisted of a glass tube with a flat quartz window at the bottom to allow for the detection of ECL. A electrochemical testing solution consisting of 0.1 M tetrabutylammonium hexafluorophosphate (TBAPF<sub>6</sub>, Sigma Aldrich)) as the supporting electrolyte in 3 mL anhydrous acetonitrile was used in conjunction with a three-electrode system consisting of a modified glassy carbon working electrode, and two coiled Pt wires which served as the counter and reference electrode, respectively. The cell was assembled in an inert Ar atmosphere.

All cyclic voltammetry and ECL experiments were conducted on a CHI 610A electrochemical workstation (CH Instruments, Austin, TX). A photomultiplier tube (PMT, R928, Hamamatsu, Japan) held at a -750 V with a high voltage power supply was used to detect the ECL generated from the electrochemical cell. The photocurrent was measured and transformed to a voltage signal using a picoammeter/voltage source (Keithley 6487, Cleveland, OH). The potential, current and photocurrent signals obtained were recorded through a LabVIEW program (National Instruments). All ECL spectra were captured using an Andor DV429-BC CCD camera cooled to -65 °C.



### 3.6 References

1. Grätzel, M., The Rise of Highly Efficient and Stable Perovskite Solar Cells. *Acc. Chem. Res.* **2017**, *50* (3), 487-491.
2. Liu, M.; Johnston, M. B.; Snaith, H. J., Efficient Planar Heterojunction Perovskite Solar Cells by Vapour Deposition. *Nature* **2013**, *501* (7467), 395-398.
3. Lin, K.; Xing, J.; Quan, L. N.; de Arquer, F. P. G.; Gong, X.; Lu, J.; Xie, L.; Zhao, W.; Zhang, D.; Yan, C.; Li, W.; Liu, X.; Lu, Y.; Kirman, J.; Sargent, E. H.; Xiong, Q.; Wei, Z., Perovskite Light-emitting Diodes with External Quantum Efficiency Exceeding 20 %. *Nature* **2018**, *562* (7726), 245-248.
4. Yong, Z.-J.; Guo, S.-Q.; Ma, J.-P.; Zhang, J.-Y.; Li, Z.-Y.; Chen, Y.-M.; Zhang, B.-B.; Zhou, Y.; Shu, J.; Gu, J.-L.; Zheng, L.-R.; Bakr, O. M.; Sun, H.-T., Doping-Enhanced Short-Range Order of Perovskite Nanocrystals for Near-Unity Violet Luminescence Quantum Yield. *J. Am. Chem. Soc.* **2018**, *140* (31), 9942-9951.
5. Ji, S.; Yuan, X.; Cao, S.; Ji, W.; Zhang, H.; Wang, Y.; Li, H.; Zhao, J.; Zou, B., Near-Unity Red  $\text{Mn}^{2+}$  Photoluminescence Quantum Yield of Doped  $\text{CsPbCl}_3$  Nanocrystals with Cd Incorporation. *J. Phys. Chem. Lett.* **2020**, *11* (6), 2142-2149.
6. Shekhirev, M.; Goza, J.; Teeter, J. D.; Lipatov, A.; Sinitskii, A., Synthesis of Cesium Lead Halide Perovskite Quantum Dots. *J. Chem. Educ.* **2017**, *94* (8), 1150-1156.
7. Liu, W.; Lin, Q.; Li, H.; Wu, K.; Robel, I.; Pietryga, J. M.; Klimov, V. I.,  $\text{Mn}^{2+}$ -Doped Lead Halide Perovskite Nanocrystals with Dual-color Emission Controlled by Halide Content. *J. Am. Chem. Soc.* **2016**, *138* (45), 14954-14961.
8. McLaurin, E. J.; Vlaskin, V. A.; Gamelin, D. R., Water-Soluble Dual-Emitting Nanocrystals for Ratiometric Optical Thermometry. *J. Am. Chem. Soc.* **2011**, *133* (38), 14978-14980.

9. Xie, R.; Peng, X., Synthesis of Cu-Doped InP Nanocrystals (d-dots) with ZnSe Diffusion Barrier as Efficient and Color-Tunable NIR Emitters. *J. Am. Chem. Soc.* **2009**, *131* (30), 10645-10651.
10. Chen, H. Y.; Chen, T. Y.; Son, D. H., Measurement of Energy Transfer Time in Colloidal Mn-Doped Semiconductor Nanocrystals. *J. Phys. Chem. C* **2010**, *114* (10), 4418-4423.
11. White, M. A.; Weaver, A. L.; Beaulac, R.; Gamelin, D. R., Electrochemically Controlled Auger Quenching of Mn<sup>2+</sup> Photoluminescence in Doped Semiconductor Nanocrystals. *ACS Nano* **2011**, *5* (5), 4158-4168.
12. Mir, W. J.; Jagadeeswararao, M.; Das, S.; Nag, A., Colloidal Mn-Doped Cesium Lead Halide Perovskite Nanoplatelets. *ACS Energy Lett.* **2017**, *2* (3), 537-543.
13. Vlaskin, V. A.; Janssen, N.; van Rijssel, J.; Beaulac, R.; Gamelin, D. R., Tunable Dual Emission in Doped Semiconductor Nanocrystals. *Nano Lett.* **2010**, *10* (9), 3670-3674.
14. Hesari, M.; Ding, Z., Review—Electrogenerated Chemiluminescence: Light Years Ahead. *J. Electrochem. Soc.* **2016**, *163* (4), H3116-H3131.
15. Richter, M. M., Electrochemiluminescence (ECL). *Chem. Rev.* **2004**, *104* (6), 3003-3036.
16. Miao, W., Electrogenerated Chemiluminescence and Its Biorelated Applications. *Chem. Rev.* **2008**, *108* (7), 2506-2553.
17. Dong, Y.; Chen, C.; Lin, J.; Zhou, N.; Chi, Y.; Chen, G., Electrochemiluminescence Emission from Carbon Quantum Dot-sulfite Coreactant System. *Carbon* **2013**, *56*, 12-17.
18. Zhang, R.; Adsetts, J. R.; Nie, Y.; Sun, X.; Ding, Z., Electrochemiluminescence of Nitrogen- and Sulfur-doped Graphene Quantum Dots. *Carbon* **2018**, *129*, 45-53.

19. Ye, S.; Sun, J.-Y.; Han, Y.-H.; Zhou, Y.-Y.; Zhang, Q.-Y., Confining Mn<sup>2+</sup>-Doped Lead Halide Perovskite in Zeolite-Y as Ultrastable Orange-Red Phosphor Composites for White Light-Emitting Diodes. *ACS Appl. Mater. Interfaces* **2018**, *10* (29), 24656-24664.
20. Chen, D.; Fang, G.; Chen, X., Silica-Coated Mn-Doped CsPb(Cl/Br)<sub>3</sub> Inorganic Perovskite Quantum Dots: Exciton-to-Mn Energy Transfer and Blue-Excitable Solid-State Lighting. *ACS Appl. Mater. Interfaces* **2017**, *9* (46), 40477-40487.
21. Tan, X.; Zhang, B.; Zou, G., Electrochemistry and Electrochemiluminescence of Organometal Halide Perovskite Nanocrystals in Aqueous Medium. *J. Am. Chem. Soc.* **2017**, *139* (25), 8772-8776.
22. Kong, Y.; Zhang, B.-H.; Zeng, Z.-H.; Zhang, Y.-W.; Niu, L., Recent Advances in Electrochemiluminescence of Halide Perovskites. *Chin. J. Anal. Chem.* **2020**, *48* (2), e20021-e20031.
23. Yadav, J.; Liang, Q.; Pan, S., Electrogenerated Chemiluminescence and Spectroelectrochemistry Characteristics of Blue Photoluminescence Perovskite Quantum Dots. *ACS Appl. Mater. Interfaces* **2020**, *12* (24), 27443-27452.
24. Samu, G. F.; Scheidt, R. A.; Kamat, P. V.; Janáky, C., Electrochemistry and Spectroelectrochemistry of Lead Halide Perovskite Films: Materials Science Aspects and Boundary Conditions. *Chem. Mater.* **2018**, *30* (3), 561-569.
25. Cai, Z.; Li, F.; Xu, W.; Xia, S.; Zeng, J.; He, S.; Chen, X., Colloidal CsPbBr<sub>3</sub> Perovskite Nanocrystal Films as Electrochemiluminescence Emitters in Aqueous solutions. *Nano Res.* **2018**, *11* (3), 1447-1455.
26. Hao, N.; Lu, J.; Dai, Z.; Qian, J.; Zhang, J.; Guo, Y.; Wang, K., Analysis of Aqueous Systems Using All-inorganic Perovskite CsPbBr<sub>3</sub> Quantum Dots with Stable Electrochemiluminescence Performance using a Closed Bipolar Electrode. *Electrochem. Commun.* **2019**, *108*, 106559.

27. Peng, H.; Wu, W.; Huang, Z.; Xu, L.; Sheng, Y.; Deng, H.; Xia, X.; Chen, W., Cathodic Electrochemiluminescence Performance of All-inorganic Perovskite CsPbBr<sub>3</sub> Nanocrystals in an Aqueous Medium. *Electrochem. Commun.* **2020**, *111*, 106667.
28. Huang, Y.; Long, X. Y.; Shen, D. Z.; Zou, G. Z.; Zhang, B.; Wang, H. S., Hydrogen Peroxide Involved Anodic Charge Transfer and Electrochemiluminescence of All-Inorganic Halide Perovskite CsPbBr<sub>3</sub> Nanocrystals in an Aqueous Medium. *Inorg. Chem.* **2017**, *56* (17), 10135-10138.
29. Huang, Y.; Fang, M. X.; Zou, G. Z.; Zhang, B.; Wang, H. S., Monochromatic and Electrochemically Switchable Electrochemiluminescence of Perovskite CsPbBr<sub>3</sub> Nanocrystals. *Nanoscale* **2016**, *8* (44), 18734-18739.
30. Qiu, L.; Lin, L.; Huang, Y.; Lai, Z.; Li, F.; Wang, S.; Lin, F.; Li, J.-F.; Wang, Y.; Chen, X., Unveiling Interfacial Electrochemiluminescence Behavior of Lead Halide Perovskite Nanocrystals. *Nanoscale Adv.* **2019**.
31. Leland, J. K., Electrogenenerated Chemiluminescence: An Oxidative-Reduction Type ECL Reaction Sequence Using Tripropyl Amine. *J. Electrochem. Soc.* **1990**, *137* (10), 3127.
32. Miao, W.; Choi, J.-P.; Bard, A. J., Electrogenenerated Chemiluminescence 69: The Tris(2,2'-bipyridine)ruthenium(II), (Ru(bpy)<sub>3</sub><sup>2+</sup>)/Tri-n-propylamine (TPrA) System Revisited A New Route Involving TPrA<sup>•+</sup> Cation Radicals. *J. Am. Chem. Soc.* **2002**, *124* (48), 14478-14485.
33. Wong, J. M.; Zhang, R.; Xie, P.; Yang, L.; Zhang, M.; Zhou, R.; Wang, R.; Shen, Y.; Yang, B.; Wang, H.-B.; Ding, Z., Revealing Crystallization Induced Blue Shift Emission of a Di-Boron Complex by Enhanced Photoluminescence and Electrochemiluminescence. *Angew. Chem. Int. Ed.* **2020**, *59* (40), 17461-17466.

34. Swanick, K. N.; Hesari, M.; Workentin, M. S.; Ding, Z., Interrogating Near-Infrared Electrogenerated Chemiluminescence of  $\text{Au}_{25}(\text{SC}_2\text{H}_4\text{Ph})_{18}^+$  Clusters. *J. Am. Chem. Soc.* **2012**, *134* (37), 15205-15208.
35. Myung, N.; Ding, Z.; Bard, A. J., Electrogenerated Chemiluminescence of CdSe Nanocrystals. *Nano Lett.* **2002**, *2* (11), 1315-1319.
36. Bard, A.; Ding, Z.; Myung, N., Electrochemistry and Electrogenerated Chemiluminescence of Semiconductor Nanocrystals in Solutions and in Films. *Struct. Bond. (Berlin)* **2005**, *118*, 1-57.
37. Ding, Z.; Quinn, B. M.; Haram, S. K.; Pell, L. E.; Korgel, B. A.; Bard, A. J., Electrochemistry and Electrogenerated Chemiluminescence from Silicon Nanocrystal Quantum Dots. *Science* **2002**, *296* (5571), 1293-1297.
38. Wang, F.; Lin, J.; Zhao, T. B.; Hu, D. D.; Wu, T.; Liu, Y., Intrinsic "Vacancy Point Defect" Induced Electrochemiluminescence from Coreless Supertetrahedral Chalcogenide Nanocluster. *J. Am. Chem. Soc.* **2016**, *138* (24), 7718-7724.
39. Protesescu, L.; Yakunin, S.; Bodnarchuk, M. I.; Krieg, F.; Caputo, R.; Hendon, C. H.; Yang, R. X.; Walsh, A.; Kovalenko, M. V., Nanocrystals of Cesium Lead Halide Perovskites ( $\text{CsPbX}_3$ , X= Cl, Br, and I): Novel Optoelectronic Materials Showing Bright Emission with Wide Color Gamut. *Nano Lett.* **2015**, *15* (6), 3692-3696.
40. Rossi, D.; Parobek, D.; Dong, Y.; Son, D. H., Dynamics of Exciton–Mn Energy Transfer in Mn-Doped  $\text{CsPbCl}_3$  Perovskite Nanocrystals. *J. Phys. Chem. C* **2017**, *121* (32), 17143-17149.
41. Zou, S.; Liu, Y.; Li, J.; Liu, C.; Feng, R.; Jiang, F.; Li, Y.; Song, J.; Zeng, H.; Hong, M.; Chen, X., Stabilizing Cesium Lead Halide Perovskite Lattice through Mn(II) Substitution for Air-Stable Light-Emitting Diodes. *J. Am. Chem. Soc.* **2017**, *139* (33), 11443-11450.

42. Parobek, D.; Roman, B. J.; Dong, Y.; Jin, H.; Lee, E.; Sheldon, M.; Son, D. H., Exciton-to-Dopant Energy Transfer in Mn-Doped Cesium Lead Halide Perovskite Nanocrystals. *Nano Lett.* **2016**, *16* (12), 7376-7380.
43. Das Adhikari, S.; Behera, R. K.; Bera, S.; Pradhan, N., Presence of Metal Chloride for Minimizing the Halide Deficiency and Maximizing the Doping Efficiency in Mn(II)-Doped CsPbCl<sub>3</sub> Nanocrystals. *J. Phys. Chem. Lett.* **2019**, *10* (7), 1530-1536.
44. Omer, K. M.; Ku, S.-Y.; Chen, Y.-C.; Wong, K.-T.; Bard, A. J., Electrochemical Behavior and Electrogenated Chemiluminescence of Star-Shaped D-A Compounds with a 1,3,5-Triazine Core and Substituted Fluorene Arms. *J. Am. Chem. Soc.* **2010**, *132* (31), 10944-10952.
45. Bard, A. J., *Electrogenated Chemiluminescence*. 1 ed.; Marcel Dekker, Inc.: New York, NW 10016, U.S.A., 2004; p 16.
46. Tokel, N. E.; Keszthelyi, C. P.; Bard, A. J., Electrogenated chemiluminescence. X.  $\alpha$ ,  $\beta$ ,  $\gamma$ ,  $\delta$ -Tetraphenylporphine Chemiluminescence. *J. Am. Chem. Soc.* **1972**, *94* (14), 4872-4877.
47. Chandross, E. A.; Sonntag, F. I., Chemiluminescent Electron-Transfer Reactions of Radical Anions. *J. Am. Chem. Soc.* **1966**, *88* (6), 1089-1096.
48. Santa Cruz, T. D.; Akins, D. L.; Birke, R. L., Chemiluminescence and Energy Transfer in Systems of Electrogenated Aromatic Anions and Benzoyl Peroxide. *J. Am. Chem. Soc.* **1976**, *98* (7), 1677-1682.
49. Qi, H.; Chen, Y.-H.; Cheng, C.-H.; Bard, A. J., Electrochemistry and Electrogenated Chemiluminescence of Three Phenanthrene Derivatives, Enhancement of Radical Stability, and Electrogenated Chemiluminescence Efficiency by Substituent Groups. *J. Am. Chem. Soc.* **2013**, *135* (24), 9041-9049.
50. Polo, F.; Rizzo, F.; Veiga-Gutierrez, M.; De Cola, L.; Quici, S., Efficient Greenish Blue Electrochemiluminescence from Fluorene and Spirobifluorene Derivatives. *J. Am. Chem. Soc.* **2012**, *134* (37), 15402-15409.

51. Liu, H.; Wu, Z.; Shao, J.; Yao, D.; Gao, H.; Liu, Y.; Yu, W.; Zhang, H.; Yang, B., CsPbxMn1-xCl3 Perovskite Quantum Dots with High Mn Substitution Ratio. *ACS Nano* **2017**, *11* (2), 2239-2247.
52. Paul, S.; Bladt, E.; Richter, A. F.; Döblinger, M.; Tong, Y.; Huang, H.; Dey, A.; Bals, S.; Debnath, T.; Polavarapu, L.; Feldmann, J., Manganese-Doping-Induced Quantum Confinement within Host Perovskite Nanocrystals through Ruddlesden-Popper Defects. *Angew. Chem. Int. Ed.* **2020**, *59* (17), 6794-6799.

## Chapter 4

### 4 Carbon Quantum Dots derived from Phytic Acid, Glucose and Phosphoric Acid

#### 4.1 Introduction

Quantum dots (QDs) are semiconducting nanoparticles that often exhibit interesting photoluminescent (PL) properties, making them interesting contenders as potential ECL luminophores. Carbon quantum dots (CQDs) have seen great attention in recent years as there is a strive towards, low-cost, biologically compatible, and easily synthesized nanomaterials.<sup>1-2</sup> CQDs have been reported to exhibit a wide emissive gamut, aggregation-induced emission phenomenon and high PL efficiencies.<sup>3-5</sup> Functionalization of CQDs has equally been a large topic of discussion, as this has been shown to alter both photophysical and electrochemical properties.<sup>6-8</sup>

Synthesis of these nanomaterials can be performed in aqueous medium, and has been shown to achieve biocompatibility.<sup>9</sup> Primarily, two synthetic methods have been largely explored. Top down methodologies employ large carbon structures that are broken down to smaller sized materials.<sup>10-11</sup> In contrast, bottom up synthesis utilizes a wide variety of molecular precursors which provides an opportune method for heteroatom incorporation.<sup>12-13</sup> Previous studies have shown that incorporation of heteroatoms into the graphene lattice of CQDs often changes their optical and electronic properties.<sup>14</sup> Therefore, it is of interest to study how the incorporation of heteroatoms into the CQD structure may affect the PL and ECL emission. ECL has long been associated with probing the surface states while PL the core emission.<sup>15</sup> It remains unclear the exact correlation between these two light emitting processes, especially in the area of quantum dot research. Previous studies in the Ding group have focused on blue emissive CQDs.<sup>16-18</sup> The CQD synthesis discussed in this chapter is aimed at procuring longer wavelength emitting nanoparticles.

#### 4.2 Synthesis of Carbon Quantum Dots (CQD)

CQDs were synthesized by utilizing a pyrolysis method. This method involves heating the solid/liquid precursors beyond the melting point and immediately quenching



the completed reaction with water. Melting is quite a facile synthetic procedure requiring approximately only five minutes to obtain luminescent nanomaterials. Due to short synthetic reaction times, multiple trials can be performed consecutively. This method utilizes phytic acid as the main carbon, oxygen and phosphorous source. An additional dopant was added to the reaction flask to provide a source of heteroatoms for incorporation into the quantum dot structure. Table 4-1 below outlines the various synthetic trials undertaken to obtain the highest PL intensity CQD. The reaction temperature was held at 240 °C for all trials and the final volume after quenching with water was held constant at 5 mL. As a result, a rough PL test can be performed by creating a sample consisting of 200  $\mu$ L from the reaction flask and diluting with 3 mL of water for each trial.

**Table 4-1.** Summary of various synthesis trials to obtain unique carbon quantum dots

Sample	Variable	Phytic Acid (g)	Phosphoric Acid (mL)	Dopant	Maximum Photoluminescence Intensity (cps)	Emission Wavelength $\lambda_{\text{max}}$ (nm)
J-1	Reaction Time (Short)	0.2	1.4	Urea - 0.2 g	100500	410
J-2	Reaction Time (Long)	0.2	1.4	Urea - 0.2 g	700000	410
J-3	Urea Quantity	0.2	1.4	Urea - 0.05 g	450000	410
J-4	Only Phytic Acid	0.2	1.4	-	10000	550
J-5	High Quantity $\text{H}_3\text{PO}_4$	0.2	2.1	-	7000	560

J-6	Low Quantity H <sub>3</sub> PO <sub>4</sub>	0.2	0.7	-	6000	560
J-7	Addition of TPrA	0.2	1.4	TPrA - 10 uL	6000	520
J-9	Glucose	0.2	1.4	Glucose – 0.1 g	100000	515

Based on the preliminary PL results, J-2 exhibited the highest photoluminescence intensity. Commonly utilized reagents in CQD synthesis include urea and citric acid which are used to produce highly blue emissive CQDs. These syntheses have been extensively reported in literature.<sup>19</sup> To study less commonly found green emissive CQDs, trial J-9 was chosen to proceed with optimization.

The synthetic procedure was optimized by varying the ratio of phytic acid to glucose. Three trials were performed where the phytic acid:glucose ratio was varied between 4:1, 2:1 and 1:2. Rough PL testing was performed in a similar manner by maintaining a constant end reaction volume and diluting a 200  $\mu$ L aliquot with 3 mL of water. The results of the optimization are outlined in Table 4-2 below.

**Table 4-2.** Summary of J-9 dopant ratio synthetic parameter optimization

Sample	Variable	Phytic Acid (g)	Phosphoric Acid (mL)	Dopant	Maximum Photoluminescence Intensity (cps)	Emission Wavelength $\lambda_{\text{max}}$ (nm)
J-9-1	Dopant Ratio	0.4	1.0	Glucose - 0.1 g	100000	515
J-9-2	Dopant Ratio	0.2	1.0	Glucose - 0.1 g	70000	515
J-9-3	Dopant Ratio	0.2	1.0	Glucose - 0.4 g	76000	515

Sample J-9-1 exhibited the best photoluminescence performance and was selected for further purification and isolation. The CQDs were synthesized by the pyrolysis and heating of glucose, phytic acid and phosphoric acid in the same reaction flask (heating to 240 °C). This synthetic method utilizes phytic acid (structure shown in Figure 4-1) as the main carbon, oxygen and phosphorous source. Additional reagents consisting of glucose and phosphoric acid (structures shown in Figure 4-1) were added to the reaction flask to provide a source of phosphorous and oxygen heteroatoms for incorporation into the quantum dot structure. The phytic acid was added at a 4:1 mass ratio to glucose (0.4 g : 0.1 g) into 1 mL of concentrated phosphoric acid and stirred until the solid was dissolved. The reaction flask was heated to 240 °C for 5.5 minutes until a thick amber liquid was obtained.

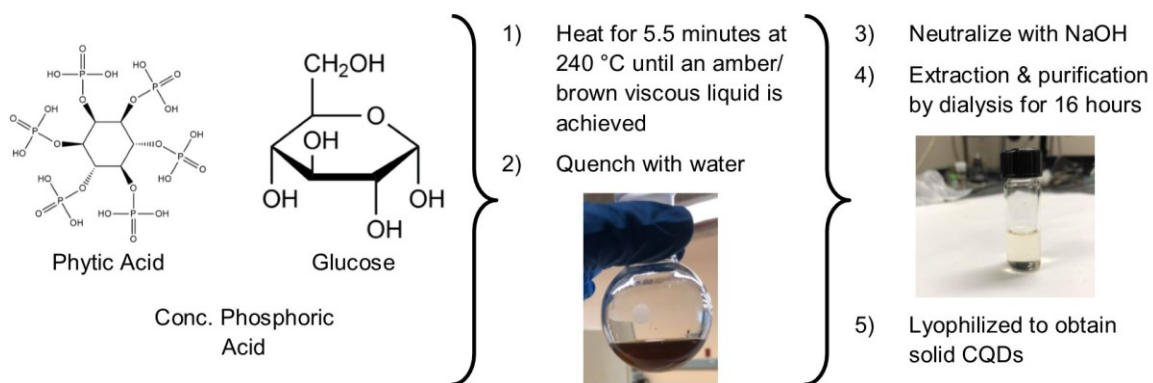


**Figure 4-1.** Synthetic procedure to synthesize new CQD from phytic acid, glucose and phosphoric acid precursors.

The reaction was then quenched upon the addition of 4 mL of Type 1 (18.2 MΩ·cm) ultrapure water. Sodium hydroxide pellets were then added into the reaction flask under sonication until a neutral pH was achieved. Ethanol was added in 2 mL increments to extract the CQD from the aqueous phase. Extraction was completed by visual inspection (absence of luminescence). The ethanol was then evaporated until a thick paste consisting of CQDs remained. Finally, the CQDs were dispersed in ultrapure water, filtered using a 0.1 μm syringe filter and dialyzed for 16 hours before undergoing freeze drying to obtain a yellow powder. A yield of 0.5493 g was obtained utilizing this synthetic procedure. By comparing the mass of the precursors and final CQD product, the percent yield was found to be around 23 %.

### 4.3 Results and Discussion

The photoluminescence properties of the CQDs were explored for the synthetic method outlined above. Optimization of the synthetic procedure involving phytic acid to glucose ratios of 4:1, 2:1, 10:1 and 1:2, each in 1 mL phosphoric acid were explored. However, only the 4:1 phytic acid to glucose ratio will be discussed further as its PL emission exhibited the highest intensity during preliminary testing. Figure 4.2 below shows the PL spectrum of the CQDs dispersed in water (0.1 g/mL) obtained from the optimized synthesis.

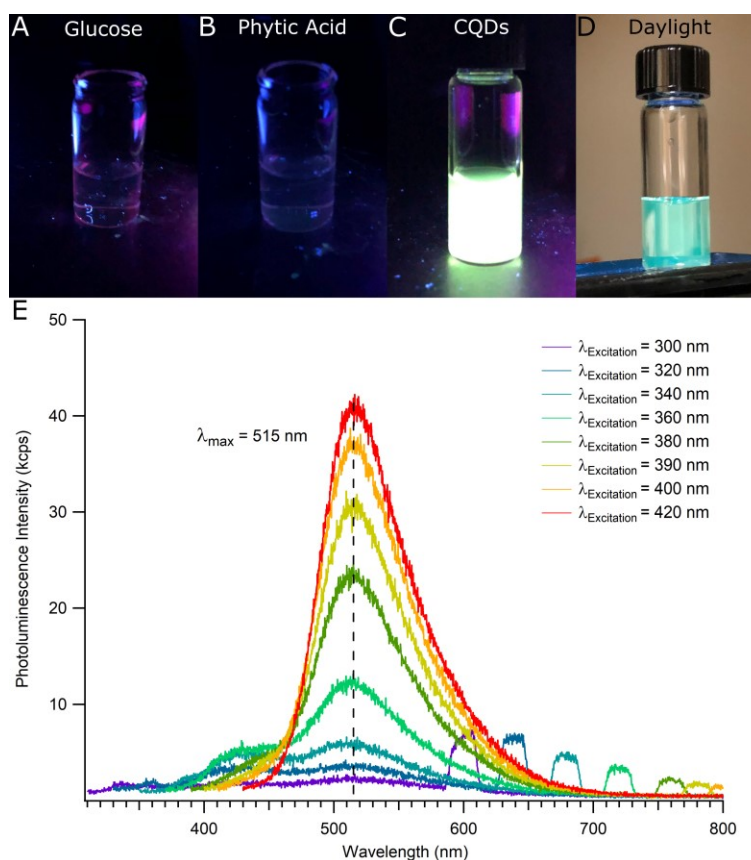


**Figure 4-2.** Fluorescence images obtained of (A) Glucose, (B) Phytic Acid, (C) Purified CQDs dispersed in water (0.1 g/mL), under a 254 nm UV lamp and (D) Purified CQDs dispersed in water (0.1 g/mL) under broad daylight. (E) PL spectra of the CQD dispersed in water (0.1 g/mL) excited at varying wavelengths from 300 to 420 nm.

Interestingly, the PL spectra display a predominant emission peak at  $\lambda_{\text{max}} = 515$  nm. The corresponding luminescence is a strong green color, as indicated by the photographs in Figure 4.2B. This emission with a  $\lambda_{\text{max}} = 515$  nm is excitation independent as the peak position remains fixed at different excitatory wavelengths. The PL quantum yield was found to be 23 % relative to quinine sulfate. This is quite interesting, as many CQDs reported in literature exhibit a blue wavelength emission, however green and longer wavelength emissive CQD remain quite rare and lucrative. Therefore, the newly synthesized CQDs are of interest to pursue further electrochemical and electrochemiluminescence studies as they exhibit a good PL efficiency.

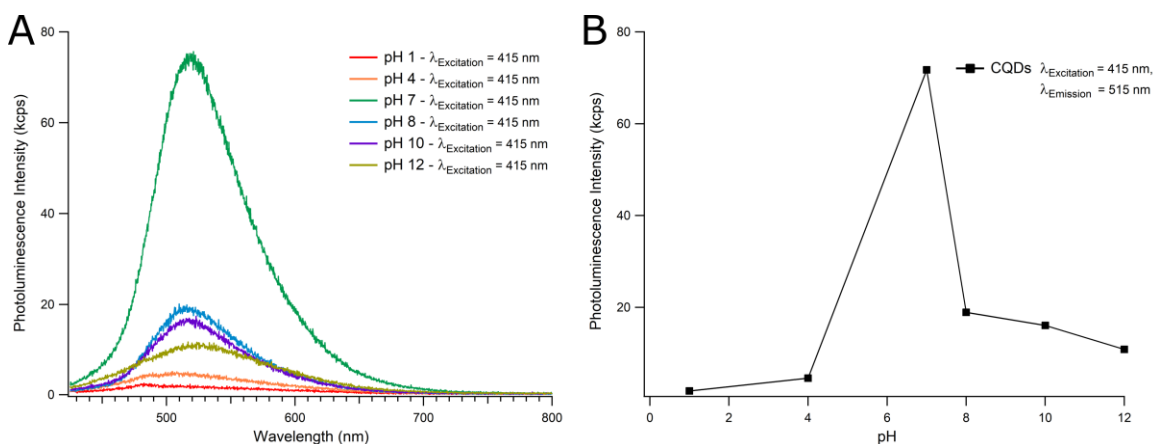


**Figure 4-3.** (A) PL spectra depicting the pH dependent nature of the CQD emission upon photoexcitation at 415 nm (0.1 g/mL). (B) Maximum PL intensity versus pH of the newly synthesized CQD taken at  $\lambda_{\text{Emission}} = 515$  nm upon photoexcitation at 415 nm (0.1 g/mL).

By subjecting the CQD to different pH solutions, PL intensity drastically changed. Figure 4-3 A displays the PL spectra obtained by dispersing the CQDs at 0.1 g/mL into buffer solutions at pH 1,4,8,10, and 12. In slightly basic conditions, the PL exhibited a nearly 4 times decrease in intensity (Figure 4-3 B). While in acidic conditions, little PL was observed for the CQD sample. Therefore, the newly synthesized CQDs exhibit a pH dependent PL emission that can be exploited towards use in pH detection applications.

Solubility tests indicate that the CQDs are only soluble in water and sparingly soluble in ethanol. Therefore, a stock solution of CQDs at a concentration of 1 g/mL was prepared and 10  $\mu$ L was drop casted onto a bare glassy carbon electrode (GCE). The

modified electrode was left to dry on the benchtop overnight. An electrochemical cell consisting of 0.1 M TBAP in 1:1 acetonitrile to water was prepared by purging with Ar with the 10 mg modified GCE as the working electrode and Pt wires serving as the counter and reference electrodes. The annihilation pathway of the CQDs was explored by first scanning towards the cathodic region (Figure 4-4 A). The CV (red trace) indicates one reduction peak present at around -2.0 V. In the scan towards the anodic region (Figure 4-4B), no oxidation peaks were observed in the CV (red trace). Therefore, it is reasonable that no ECL can be generated in the annihilation pathway as the radical cation species is not accessible in this system's potential window.

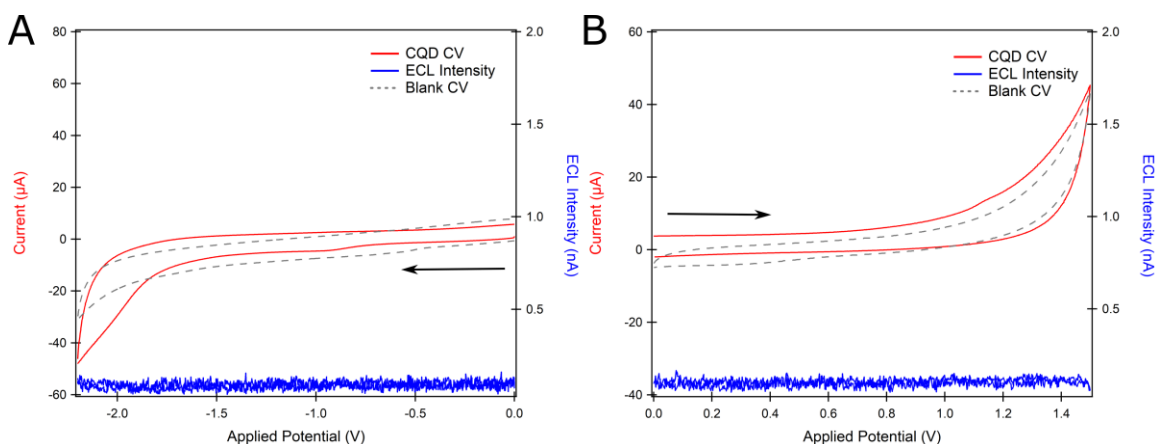


**Figure 4-4.** (A) Cyclic voltammogram of the CQDs – red trace, blank – dotted line, and the corresponding ECL voltage curve – blue trace upon scanning towards the cathodic region. (B) Cyclic voltammogram of the CQDs – red trace, blank – dotted line, and the corresponding ECL voltage curve – blue trace upon scanning towards the anodic region.

As no ECL was generated in the annihilation pathway, benzoyl peroxide (BPO) was added as a coreactant to induce excited state formation from the radical anion species. Upon the addition of 5 mM BPO to the solution, 4 nA was obtained as noted by the ECL-voltage curve (blue trace) in Figure 4-5 A. In the scan towards the cathodic region, BPO is first reduced at around -1.0 V and then at a further negative potential, CQD reduction is observed at -2.0 V in the CV (red trace). The elucidation of ECL occurs at around -1.8 V which matches well with the reduction potential of the CQD. Therefore, the ECL observed

in the BPO coreactant pathway is attributed to the formation of the CQD\* excited state species.

Since the electrochemical profile of quantum dots is not always easily observed by CV, the coreactant tri-propylamine (TPrA) was added to confirm the absence of the radical cation CQD species. Figure 4-5 B indicates the CV and corresponding ECL-voltage curve upon the addition of 20 mM TPrA. At around 0.8 V, TPrA oxidation occurs, however no ECL is generated upon scanning further positive. Therefore, this confirms that the CQD cannot be oxidized within the solvent potential window (Figure 4-4 B).

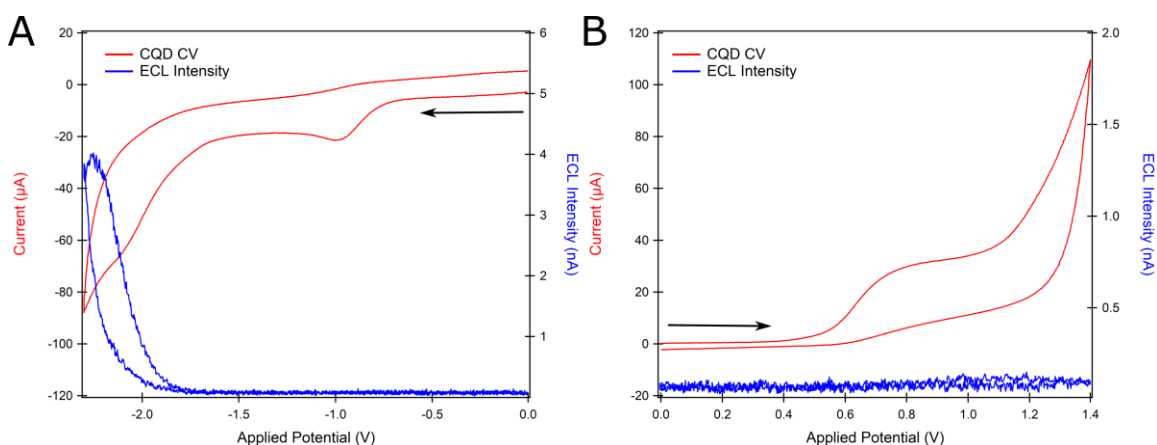
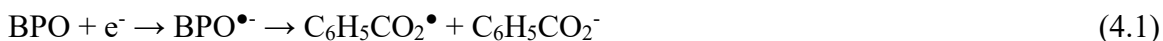


**Figure 4-5.** Cyclic voltammogram of the CQD – red trace and corresponding ECL-voltage curve (blue trace) of a 10 mg modified GCE in 1:1 water:acetonitrile solution with 0.1 M TBAP as the supporting electrolyte with (A) 5 mM BPO and (B) 20 mM TPrA as the coreactant.

Due to the low ECL intensity of the CQD in the coreactant pathway, no spectrum was obtained. Although the ECL wavelength could not be confirmed, the proposed mechanism for generating the excited state species is outlined below.





BPO is first reduced upon scanning towards the cathodic region, and consequently cleaves to form the benzoate radical ( $\text{C}_6\text{H}_5\text{CO}_2^\bullet$ ) and benzoate anion (Eq. 4.1). Then CQD is reduced upon scanning further negative to form  $\text{CQD}^{\bullet-}$  species (Eq. 4.2). Once the  $\text{CQD}^{\bullet-}$  is produced in the film, it can undergo an electron transfer reaction with the benzoate radical present in the solution to form the  $\text{CQD}^*$  excited state species (Eq. 4.3). This excited state species can then relax and emit light (Eq. 4.4).

Although ECL tests are currently inconclusive, there remain many different avenues that can be explored in the future. Accessing the  $\text{CQD}/\text{CQD}^{\bullet-}$  reduction potential while maintaining good compatibility between solvent systems and coreactant can be explored in the future. Secondly, functionalization of the CQD or post-synthetic treatments may alter its electrochemical profile as well as its light emitting properties. Therefore, studies can be performed to investigate how functionalization of the CQD post-synthesis can shift the reduction potential to one that is less negative to easily generate the radical anion species. Nonetheless, a promising new CQD derived from glucose, phytic acid and phosphoric acid was synthesized that exhibits a green colored emission with a quantum yield of 23 % relative to quinine sulfate. The CQDs were shown to have an excitation-independent emission, as the emission  $\lambda_{\text{max}}$  remains unchanged at varying excitation wavelengths. Furthermore, pH was shown to have a substantial effect on the PL intensity. ECL and electrochemical experiments confirmed the presence of a reduction event occurring at -2.0 V with a maximum of 4 nA ECL generated upon the addition of 5 mM BPO.

## 4.4 Experimental

D-Glucose ( $\text{C}_6\text{H}_{12}\text{O}_6$ , Alfa Aesar), phytic acid ( $\text{C}_6\text{H}_{18}\text{O}_{24}\text{P}_6$ , Sigma Aldrich) and phosphoric acid ( $\text{H}_3\text{PO}_4$ , Anachemia) were used in the synthesis of CQD. Sodium hydroxide pellets ( $\text{NaOH}$ , Alfa Aesar) and 95 % ethanol ( $\text{EtOH}$ ) were used in the extraction stages. Ultrapure type 1 ( $18.2 \text{ M}\Omega \cdot \text{cm}$ ) was used in all stages of purification and synthesis. Dialysis bags with a 1000 Da molecular weight cut off (Shanghai Yuanye Bio-Technology



Co. Ltd) and Whatman 0.1  $\mu\text{m}$  syringe filters (Millipore Sigma) were used during the final purification steps.

The UV-visible absorbance spectra were obtained on a Varian Cary – 50 spectrophotometer. Photoluminescence experiments were performed on a Fluorolog instrument (QM-7/2005, Photon Technology International) with an excitation slit width of 0.25 au and an emission slit width of 0.1 au. Photoluminescence experiments involving pH dependent emission studies utilized CQD prepared in aqueous buffer solutions of varying pH. Buffer solutions at pH 1, 4, 8, 10 and 12 (Fisher Chemical) were used to make 0.1 g/mL CQD samples for PL testing.

An electrochemical cell was utilized for cyclic voltammetry and subsequent ECL studies. The electrochemical cell consisted of a glass tube with a flat Pyrex window at the bottom to allow for the detection of ECL. A solution for electrochemical testing was made consisting of 0.1 M tetrabutylammonium perchlorate (TBAP, Sigma Aldrich) as the supporting electrolyte in 3 mL of 1:1 water:acetonitrile. A three-electrode system consisting of a modified glassy carbon working electrode, and two coiled Pt wires which served as the counter and reference electrode, respectively. The cell was purged with Ar gas for 30 minutes before performing electrochemical studies.

All cyclic voltammetry and ECL experiments were conducted on a CHI 610A electrochemical workstation (CH Instruments, Austin, TX). A photomultiplier tube (PMT, R928, Hamamatsu, Japan) held at a -750 V with a high voltage power supply was used to detect the ECL generated from the electrochemical cell. The photocurrent was measured and transformed to a voltage signal using a picoammeter/voltage source (Keithley 6487, Cleveland, OH). The potential, current and photocurrent signals obtained were recorded through a LabVIEW program (National Instruments).

## 4.5 References

1. Xu, X.; Ray, R.; Gu, Y.; Ploehn, H. J.; Gearheart, L.; Raker, K.; Scrivens, W. A., Electrophoretic Analysis and Purification of Fluorescent Single-Walled Carbon Nanotube Fragments. *J. Am. Chem. Soc.* **2004**, *126* (40), 12736-12737.
2. Hu, C.; Li, M.; Qiu, J.; Sun, Y.-P., Design and Fabrication of Carbon Dots for Energy Conversion and Storage. *Chem. Soc. Rev.* **2019**, *48* (8), 2315-2337.
3. Guo, R.; Li, T.; Shi, S., Aggregation-induced Emission Enhancement of Carbon Quantum Dots and Applications in Light Emitting Devices. *J. Mater. Chem. C* **2019**, *7* (17), 5148-5154.
4. Yuan, F.; Yuan, T.; Sui, L.; Wang, Z.; Xi, Z.; Li, Y.; Li, X.; Fan, L.; Tan, Z. a.; Chen, A.; Jin, M.; Yang, S., Engineering Triangular Carbon Quantum Dots with Unprecedented Narrow Bandwidth Emission for Multicolored LEDs. *Nat. Commun.* **2018**, *9* (1), 2249.
5. Yang, H.; Liu, Y.; Guo, Z.; Lei, B.; Zhuang, J.; Zhang, X.; Liu, Z.; Hu, C., Hydrophobic Carbon Dots with Blue Dispersed Emission and Red Aggregation-induced Emission. *Nat. Commun.* **2019**, *10* (1), 1789.
6. Dong, Y.; Wang, R.; Li, H.; Shao, J.; Chi, Y.; Lin, X.; Chen, G., Polyamine-Functionalized Carbon Quantum Dots for Chemical Sensing. *Carbon* **2012**, *50* (8), 2810-2815.
7. Farshbaf, M.; Davaran, S.; Rahimi, F.; Annabi, N.; Salehi, R.; Akbarzadeh, A., Carbon Quantum Dots: Recent Progresses on Synthesis, Surface Modification and Applications. *Artif. Cells Nanomed. Biotechnol.* **2018**, *46* (7), 1331-1348.
8. Huang, X.; Zhang, H.; Zhao, J.; Jiang, D.; Zhan, Q., Carbon Quantum Dot (CQD)-Modified Bi<sub>3</sub>O<sub>4</sub>Br Nanosheets Possessing Excellent Photocatalytic Activity Under Simulated Sunlight. *Mater. Sci. Semicond. Process.* **2021**, *122*, 105489.

9. Wang, L.; Wang, Y.; Xu, T.; Liao, H.; Yao, C.; Liu, Y.; Li, Z.; Chen, Z.; Pan, D.; Sun, L.; Wu, M., Gram-scale Synthesis of Single-crystalline Graphene Quantum Dots with Superior Optical Properties. *Nat. Commun.* **2014**, *5* (1), 5357.
10. Tan, X.; Li, Y.; Li, X.; Zhou, S.; Fan, L.; Yang, S., Electrochemical Synthesis of Small-sized Red Fluorescent Graphene Quantum Dots as a Bioimaging Platform. *Chem. Commun.* **2015**, *51* (13), 2544-2546.
11. Chu, K.; Adsetts, J. R.; He, S.; Zhan, Z.; Yang, L.; Wong, J. M.; Love, D. A.; Ding, Z., Electrogenenerated Chemiluminescence and Electroluminescence of N-Doped Graphene Quantum Dots Fabricated from an Electrochemical Exfoliation Process in Nitrogen-Containing Electrolytes. *Chem. Eur. J.* **2020**, *26* (68), 15756.
12. Peng, H.; Travas-Sejdic, J., Simple Aqueous Solution Route to Luminescent Carbogenic Dots from Carbohydrates. *Chem. Mater.* **2009**, *21* (23), 5563-5565.
13. Naik, V.; Zantye, P.; Gunjal, D.; Gore, A.; Anbhule, P.; Kowshik, M.; Bhosale, S. V.; Kolekar, G., Nitrogen-Doped Carbon Dots via Hydrothermal Synthesis: Naked Eye Fluorescent Sensor for Dopamine and Used for Multicolor Cell Imaging. *ACS Appl. Bio Mater.* **2019**, *2* (5), 2069-2077.
14. Đorđević, L.; Arcudi, F.; Prato, M., Preparation, Functionalization and Characterization of Engineered Carbon Nanodots. *Nat. Protoc.* **2019**, *14* (10), 2931-2953.
15. Ding, Z.; Quinn, B. M.; Haram, S. K.; Pell, L. E.; Korgel, B. A.; Bard, A. J., Electrochemistry and Electrogenenerated Chemiluminescence from Silicon Nanocrystal Quantum Dots. *Science* **2002**, *296* (5571), 1293-1297.
16. Zhang, R.; Adsetts, J. R.; Nie, Y.; Sun, X.; Ding, Z., Electrochemiluminescence of Nitrogen- and Sulfur-doped Graphene Quantum Dots. *Carbon* **2018**, *129*, 45-53.
17. Adsetts, J. R.; Zhang, R.; Yang, L.; Chu, K.; Wong, J. M.; Love, D. A.; Ding, Z., Efficient White Electrochemiluminescent Emission From Carbon Quantum Dot Films. *Front. Chem.* **2020**, *8* (865).

18. He, S.; Turnbull, M. J.; Nie, Y.; Sun, X.; Ding, Z., Band Structures of Blue Luminescent Nitrogen-doped Graphene Quantum Dots by Synchrotron-based XPS. *Surf. Sci.* **2018**, *676*, 51-55.
19. Sendão, R.; Yuso, M. d. V. M. d.; Algarra, M.; Esteves da Silva, J. C. G.; Pinto da Silva, L., Comparative Life Cycle Assessment of Bottom-up Synthesis Routes for Carbon Dots Derived from Citric Acid and Urea. *J. Clean. Prod.* **2020**, *254*, 120080.

## Chapter 5

### 5 Conclusions and Future Work

#### 5.1 Conclusions

In this thesis, three new materials were investigated and their photophysical properties as they pertain to the field of ECL were explored.

In Chapter 2, a newly synthesized di-boron complex displaying high promise towards use as a solid-state emitter was examined. Crystallization induced blue shift ECL was observed in the annihilation pathway of the di-boron complex film. However, a red-shifted ECL emission upon the addition of a coreactant leads to the conclusion that only the layer of molecules present at the solid/solution interface can interact with BPO to produce the excited state species and emit light. As a result, this layer of molecules is not well confined in the crystal lattice and the effects of crystallization-induced emission are difficult to observe. This work is a testament to the strength of ECL as a light emitting technique and as a method to understand and test new solid-state luminophores. The effects of crystallization-induced emission were observed and the ECL mechanism was elucidated utilizing PL spectroscopy and spooling ECL spectroscopy.

In Chapter 3, cesium lead halide perovskites, an emerging nanomaterial, were explored. Specifically,  $\text{CsPbCl}_3$  and Mn doped  $\text{CsPbCl}_3$  perovskites were investigated to elucidate the effects of Mn doping on the ECL. Based on the electrochemical profile, it was deduced that annihilation of Mn-doped  $\text{CsPbCl}_3$  radical ions proceeds via an energy insufficient pathway and generation of the excited state species is yielded by triplet-triplet annihilation. Inconsistency in spectral data and peaks that arises from curve fitting alludes to the notion that a dual emissive channel is present for the ECL of Mn-doped  $\text{CsPbCl}_3$ . The mechanism for ECL emission was then hypothesized based on the spectral evidence obtained by comparing both the undoped and Mn-doped  $\text{CsPbCl}_3$  quantum dots. The relaxation of the excited state species for the undoped  $\text{CsPbCl}_3$  leads to a 660 nm emission which is in agreement with that obtained by curve fitting the Mn-doped  $\text{CsPbCl}_3$ . As a

result, a competitive emission pathway between energy transfer to the Mn-dopant and relaxation to surface states of the quantum dot is seen in the ECL of Mn-doped CsPbCl<sub>3</sub>.

Finally, in Chapter 4, we explored the development, synthesis and preliminary testing of new CQD utilizing glucose, phytic acid and phosphoric acid as precursors. A simple 5.5-minute synthetic method was developed for obtaining the CQD. Extraction and purification methodologies were developed which lead to green emissive CQDs with a quantum yield of 23 % relative to quinine sulfate. Furthermore, the CQDs exhibit a pH dependent emission where the PL decreases 4 fold in slightly acidic or basic conditions. It was discovered that upon the addition of 5 mM BPO, ECL is generated in the cathodic region. Although the electrochemical and ECL testing is preliminary, the ability to yield a consistent green emissive wavelength ( $\lambda_{\text{max}}$ ) regardless of excitation wavelength and observance of ECL is promising for CQDs as a low-cost luminophore.

## 5.2 Future Work and Remarks

There remains an endless avenue of future work that pertains to ECL. As highlighted in Chapter 2, the BPO coreactant pathway has yet to be fully developed. The discoveries of new nanomaterials that exhibit AIE and CIE effects requires a compatible testing system to fully observe their ECL effects. As a result, further work must be done in studying the interaction between coreactant and ECL luminophores especially in the solid-state ECL system where light is generated primarily at the solid/solution interface. In Chapter 3, we briefly discuss and shed light onto ECL surface state emission of quantum dots. However, this topic remains in its infancy, as many aspects are unclear. Future work will rely heavily on the design and engineering of quantum dot nanomaterials with varying defined surface states. Consequently, ECL testing of these quantum dots, will hopefully bring forth new insights into this grey area. Finally, since the recent discovery of carbon quantum dots and their diversity, they have been an excellent contender as an ECL luminophore. Chapter 4 displays a glimpse into the vast field of carbon quantum dots and future work would involve refining and controlling the synthetic processes to achieve desired photophysical properties. As well, utilizing post-processing techniques to functionalize and expand their applications should be further explored.

The field of ECL has been developing at an incredible rate. Not only has this technique seen applications as an analytical technique, we observe its incorporation in solid-state emitting devices (light emitting electrochemical cells). However, superseding its applications, new nanomaterials are constantly appearing with interesting and complex photophysical properties. ECL is indeed a light emitting technique that is very capable in realizing these properties, however, special attention must be given to spectroscopy. In a field where high efficiencies can sometimes overshadow the fundamental investigation of the light emission mechanism; we must first understand the ramifications of electrochemical excitation and consequent emission. By connecting these processes to new nanomaterials, it will allow us to further progress the field of ECL.

## List of Appendices

**Appendix A: Reproduction permission for the paper “Revealing Crystallization Induced Blue Shift Emission of a Di-Boron Complex by Enhanced Photoluminescence and Electrochemiluminescence”**



---

This Agreement between Mr. Jonathan Wong ("You") and John Wiley and Sons ("John Wiley and Sons") consists of your license details and the terms and conditions provided by John Wiley and Sons and Copyright Clearance Center.

License Number 4925610998372

License date Oct 10, 2020

Licensed Content Publisher John Wiley and Sons

Licensed Content Publication Angewandte Chemie

Licensed Content Title Revealing Crystallization-Induced Blue-Shift Emission of a Di-Boron Complex by Enhanced Photoluminescence and Electrochemiluminescence

Licensed Content Author Jonathan M. Wong, Ruizhong Zhang, Peidong Xie, et al

Licensed Content Date Aug 11, 2020

Licensed Content Volume 132

Licensed Content Issue 40

Licensed Content Pages	6
Type of use	Dissertation/Thesis
Requestor type	Author of this Wiley article
Format	Print and electronic
Portion	Full article
Will you be translating?	No
Title	Master's Thesis
Institution name	Western University
Expected presentation date	Dec 2020

## Terms and Conditions

- The materials you have requested permission to reproduce or reuse (the "Wiley Materials") are protected by copyright.
- You are hereby granted a personal, non-exclusive, non-sub licensable (on a stand-alone basis), non-transferable, worldwide, limited license to reproduce the Wiley Materials for the purpose specified in the licensing process. This license, **and any CONTENT (PDF or image file) purchased as part of your order**, is for a one-time use only and limited to any maximum distribution number specified in the license. The first instance of republication or reuse granted by this license must be completed within two years of the date of the grant of this license (although copies prepared before the end date may be distributed thereafter). The Wiley Materials shall not be used in any other manner or for any other purpose, beyond what is granted in the license. Permission is granted subject to an appropriate acknowledgement given to the author, title of the material/book/journal and the publisher. You shall also duplicate the copyright notice that appears in the Wiley publication in your use of the Wiley Material. Permission is also granted on the understanding that nowhere in the text is a previously published source acknowledged for all or part of this Wiley Material. Any third party content is expressly excluded from this permission.
- With respect to the Wiley Materials, all rights are reserved. Except as expressly granted by the terms of the license, no part of the Wiley Materials may be copied, modified, adapted (except for minor reformatting required by the new Publication), translated, reproduced, transferred or distributed, in any form or by any means, and no derivative works may be made based on the Wiley Materials without the prior permission of the respective copyright owner. **For STM Signatory Publishers clearing permission under the terms of the STM Permissions Guidelines only, the terms of the license are extended to include subsequent editions and for editions in other languages, provided such editions are for the work as a whole in situ and does not involve the separate exploitation of the permitted figures or extracts**, You may not alter, remove or suppress in any manner any copyright, trademark or other notices displayed by the Wiley Materials. You may not license, rent, sell, loan, lease, pledge, offer as security, transfer or assign the Wiley Materials on a stand-alone basis, or any of the rights granted to you hereunder to any other person.
- The Wiley Materials and all of the intellectual property rights therein shall at all times remain the exclusive property of John Wiley & Sons Inc, the Wiley Companies, or their respective licensors, and your interest therein is only that of having possession of and the right to reproduce the Wiley Materials pursuant to Section 2 herein during the continuance of this Agreement. You agree that you own no right, title or interest in or to the Wiley Materials or any of the intellectual property rights therein. You shall have no rights hereunder other than the license as provided for above in Section 2. No right,

license or interest to any trademark, trade name, service mark or other branding ("Marks") of WILEY or its licensors is granted hereunder, and you agree that you shall not assert any such right, license or interest with respect thereto

- NEITHER WILEY NOR ITS LICENSORS MAKES ANY WARRANTY OR REPRESENTATION OF ANY KIND TO YOU OR ANY THIRD PARTY, EXPRESS, IMPLIED OR STATUTORY, WITH RESPECT TO THE MATERIALS OR THE ACCURACY OF ANY INFORMATION CONTAINED IN THE MATERIALS, INCLUDING, WITHOUT LIMITATION, ANY IMPLIED WARRANTY OF MERCHANTABILITY, ACCURACY, SATISFACTORY QUALITY, FITNESS FOR A PARTICULAR PURPOSE, USABILITY, INTEGRATION OR NON-INFRINGEMENT AND ALL SUCH WARRANTIES ARE HEREBY EXCLUDED BY WILEY AND ITS LICENSORS AND WAIVED BY YOU.
- WILEY shall have the right to terminate this Agreement immediately upon breach of this Agreement by you.
- You shall indemnify, defend and hold harmless WILEY, its Licensors and their respective directors, officers, agents and employees, from and against any actual or threatened claims, demands, causes of action or proceedings arising from any breach of this Agreement by you.
- IN NO EVENT SHALL WILEY OR ITS LICENSORS BE LIABLE TO YOU OR ANY OTHER PARTY OR ANY OTHER PERSON OR ENTITY FOR ANY SPECIAL, CONSEQUENTIAL, INCIDENTAL, INDIRECT, EXEMPLARY OR PUNITIVE DAMAGES, HOWEVER CAUSED, ARISING OUT OF OR IN CONNECTION WITH THE DOWNLOADING, PROVISIONING, VIEWING OR USE OF THE MATERIALS REGARDLESS OF THE FORM OF ACTION, WHETHER FOR BREACH OF CONTRACT, BREACH OF WARRANTY, TORT, NEGLIGENCE, INFRINGEMENT OR OTHERWISE (INCLUDING, WITHOUT LIMITATION, DAMAGES BASED ON LOSS OF PROFITS, DATA, FILES, USE, BUSINESS OPPORTUNITY OR CLAIMS OF THIRD PARTIES), AND WHETHER OR NOT THE PARTY HAS BEEN ADVISED OF THE POSSIBILITY OF SUCH DAMAGES. THIS LIMITATION SHALL APPLY NOTWITHSTANDING ANY FAILURE OF ESSENTIAL PURPOSE OF ANY LIMITED REMEDY PROVIDED HEREIN.
- Should any provision of this Agreement be held by a court of competent jurisdiction to be illegal, invalid, or unenforceable, that provision shall be deemed amended to achieve as nearly as possible the same economic effect as the original provision, and the legality, validity and enforceability of the remaining provisions of this Agreement shall not be affected or impaired thereby.
- The failure of either party to enforce any term or condition of this Agreement shall not constitute a waiver of either party's right to enforce each and every term and condition of this Agreement. No breach under this agreement shall be deemed waived or excused by either party unless such waiver or consent is in writing signed by the party granting such waiver or consent. The waiver by or consent of a party to a breach of any provision of this Agreement shall not operate or be construed as a waiver of or consent to any other or subsequent breach by such other party.
- This Agreement may not be assigned (including by operation of law or otherwise) by you without WILEY's prior written consent.

### Creative Commons Attribution-Non-Commercial-NoDerivs License

The [Creative Commons Attribution Non-Commercial-NoDerivs License \(CC-BY-NC-ND\)](#) permits use, distribution and reproduction in any medium, provided the original work is properly cited, is not used for commercial purposes and no modifications or adaptations are made. (see below)

### Use by commercial "for-profit" organizations

Use of Wiley Open Access articles for commercial, promotional, or marketing purposes requires further explicit permission from Wiley and will be subject to a fee.

Further details can be found on Wiley Online Library  
<http://olabout.wiley.com/WileyCDA/Section/id-410895.html>

### Other Terms and Conditions:

v1.10 Last updated September 2015

Questions? [customer care@copyright.com](mailto:customer care@copyright.com) or +1-855-239-3415 (toll free in the US) or +1-978-646-2777.

---

## Appendix B: Supporting Information for the paper “Revealing Crystallization Induced Blue Shift Emission of a Di-Boron Complex by Enhanced Photoluminescence and Electrochemiluminescence”

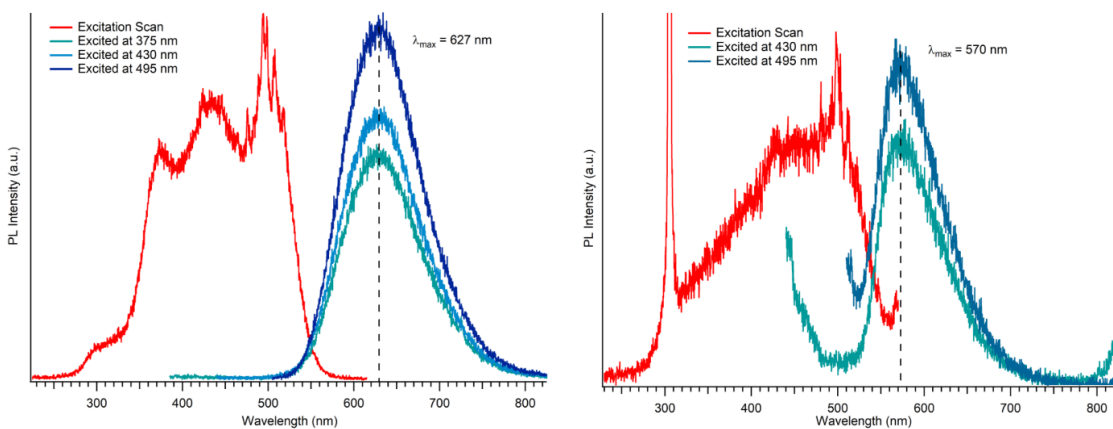


**Figure B1.** (Left panel) Excitation spectrum with a detection wavelength at 627 nm and

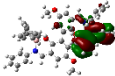
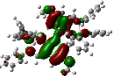
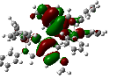
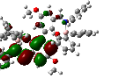
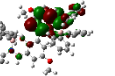
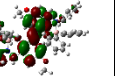
emission spectra excited at 375 nm, 430 nm and 495 nm, of a 0.25 mM DBC in acetonitrile. (Right panel) Excitation spectrum with a detection wavelength at 570 nm and emission spectra excited at 430 nm and 495 nm of a DBC crystalline film.

ECL efficiency ( $\Phi_{ECL}$ ) of the DBC was calculated with respect to a 0.25 mM  $[\text{Ru}(\text{bpy})_3]^{2+}$  standard as outlined by the equation B1 below:

$$\Phi_{ECL} = 100 \times \left( \frac{\int_a^b ECL dt}{\int_a^b \text{Current} dt} \right)_{\text{sample}} / \left( \frac{\int_a^b ECL dt}{\int_a^b \text{Current} dt} \right)_{\text{standard}} \quad (\text{B1})$$

By integrating the ECL intensities and current (charge) of the DBC film and DBC solution, a ratio between the ECL and charge generated can be obtained. By comparing this ratio to the well-established  $[\text{Ru}(\text{bpy})_3]^{2+}$  standard, a corresponding  $\Phi_{ECL}$  can be calculated.

**Table B1.** Summary of HOMO/LUMO calculations performed through DFT and electrochemistry of the DBC. DFT calculations, images and values were performed and obtained by Y. Shen and B. Yang of the State Key Lab of Supramolecular Structure and Materials at Jilin University

	HOMO-2	HOMO-1	HOMO	LUMO	LUMO+1	LUMO+2
DFT	-5.98 eV	-5.39 eV	-5.12 eV	-2.11 eV	-2.02 eV	-0.54 eV
CV	(SCE)	1.57 V	1.42 V	-1.43 V	-1.61 V	
Calc.		-5.98 eV	-5.82 eV	-2.97 eV	-2.79 eV	
						

Approximations in the calculated HOMO/LUMO energies from the CV obtained experimentally were performed with the following two equations (B2 and B3) as previously reported in reference to ferrocene.<sup>1</sup>

$$E(HOMO) = -e[E_{ox}^{onset} + 4.4] \quad (B2)$$

$$E(LUMO) = -e[E_{red}^{onset} + 4.4] \quad (B3)$$

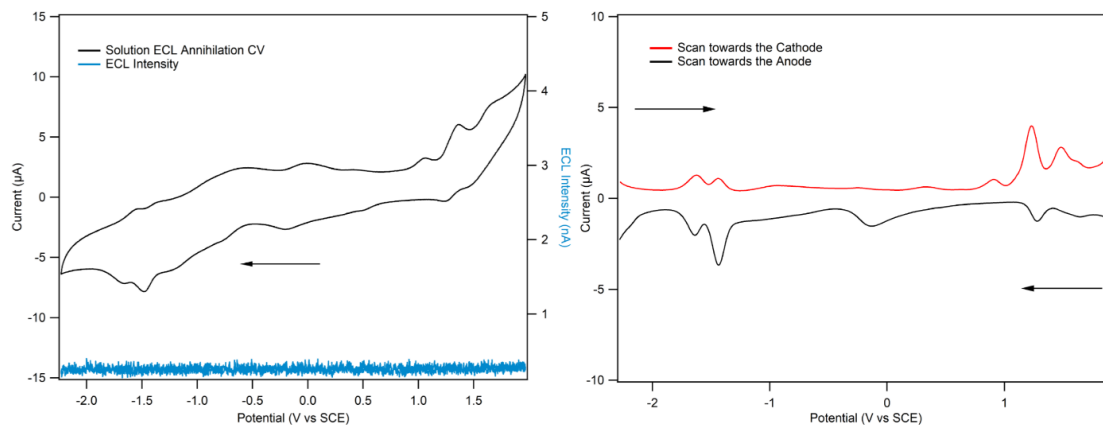


**Figure B2.** (Left panel) Cyclic voltammogram and corresponding ECL-voltage curve and (Right panel) differential pulse voltammogram of a 0.25 mM solution of DBC in acetonitrile with 0.1 M TBAP as the supporting electrolyte. A glassy carbon electrode was employed as the working electrode with one platinum wire as the reference and one platinum wire as counter electrode.

1. L. Leonat, S. Beatrice Gabriela, I. V. Brañzoi, *UPB Scientific Bulletin, Series B: Chemistry and Materials Science* **2013**, 75, 111-118.

## Curriculum Vitae

**Name:** Jonathan Michael Wong

**Post-secondary Education and Degrees:** The University of Western Ontario  
London, Ontario, Canada  
2014-2018 B.Sc. Honors in Chemistry

The University of Western Ontario  
London, Ontario, Canada  
2018-2020 M.Sc. Physical & Analytical Chemistry

**Honours and Awards:** Ontario Graduate Scholarship  
2019-2020

Natural Science and Engineering Research Council (NSERC)  
Canadian Graduate Scholarship - Masters  
2018-2019

Queen Elizabeth II Graduate Scholarship in  
Science and Technology  
2018 (declined in lieu of CGS-M)

Western Graduate Research Scholarship  
2018-2020

Canadian Institute of Chemistry – Analytical Division  
Undergraduate Travel Award  
2018

**Related Work Experience** Teaching Assistant  
The University of Western Ontario  
2018-2020

**Publications:**

“Discovering the Link between the Electrochemiluminescence and Energy Transfers/Surface States of Mn-Doped CsPbCl<sub>3</sub> Perovskites” Jonathan M. Wong, Jie Xu, Ruizhong Zhang, Kenneth Chu, Lijia Liu and Zhifeng Ding, **2020**, manuscript in preparation.



“Revealing Crystallization Induced Blue-Shift Emission of a Di-Boron Complex by Enhanced Photoluminescence and Electrochemiluminescence” Jonathan M. Wong, Ruizhong Zhang, Peidong Xie, Liqing Yang, Minlin Zhang, Ruixue Zhou, Ruiyao Wang, Yue Shen, Bing Yang, Hong-Bo Wang, and Zhifeng Ding, *Angew. Chem. Int. Ed.* **2020**, *59*, 17461.

“Electrogenerated Chemiluminescence and Electroluminescence of N-Doped graphene Quantum Dots Fabricated from an Electrochemical Exfoliation Process in Nitrogen-Containing Electrolytes” Kenneth Chu, Jonathan R. Adsetts, Shuijian He, Ziyang Zhan, Liqing Yang, Jonathan M. Wong, David A. Love, and Zhifeng Ding, *Chem. Eur. J.* **2020**, DOI: 10.1002/chem.202003395

“Efficient White Electrochemiluminescent Emission from Carbon Quantum Dot Films” Jonathan R. Adsetts, Ruizhong Zhang, Liqing Yang, Kenneth Chu, Jonathan M. Wong, David A. Love, and Zhifeng Ding, *Front. Chem.* **2020**, (8), 865.

“Benzosiloles with Crystallization-Induced Emission Enhancement of Electrochemiluminescence: Synthesis, Electrochemistry and Crystallography” Liqing Yang, Donghyun Koo, Jackie Wu, Jonathan M. Wong, Tyler Day, Ruizhong Zhang, Harshana Kologoda, Kehan Liu, Jian Wang, Zhifeng Ding, and Brian L. Pagenkopf, *Chem. Eur. J.* **2020**, *26*, 11715.

“Electrochemiluminescence of bare glassy carbon with benzoyl peroxide as the coreactant in N,N-dimethylformamide” Shuijian He, Kenneth Chu, Jonathan M. Wong, Liqing Yang, Jonathan R. Adsetts, Ruizhong Zhang, Yanhua Chen, and Zhifeng Ding, *J. Anal. Test.* **2020**, *4*, 257.

“Probing the CZTS/CdS Heterojunction Utilizing Photoelectrochemistry and X-ray Absorption Spectroscopy” Matthew J. Turnbull, Daniel Vaccarello, Jonathan M. Wong, Yun Mui Yiu, Tsun-Kong Sham, and Zhifeng Ding, *J. Chem. Phys.* **2018**, *148*, 134702.

“The effects of long duration chronic exposure to hexavalent chromium on single live cells interrogated by scanning electrochemical microscopy” Fraser P. Filice, Michelle S.M. Li, Jonathan M. Wong, and Zhifeng Ding, *J. Inorg. Biochem.* **2018**, *182*, 222.

### Conference Presentations:

“Generating Enhanced Electrochemiluminescence of Phenyl substituted Diboron Complexes” Jonathan M. Wong, Ruizhong Zhang, Liqing Yang, Hong-Bo Wang, and Zhifeng Ding, 102<sup>nd</sup> Canadian Chemistry Conference, Quebec City, Quebec. June 06, **2019**.

“Comparing the effects of trivalent and hexavalent chromium on single live cells using SECM” Jonathan M. Wong, Fraser P. Filice, Michelle S.M. Li, and Zhifeng Ding, 7<sup>th</sup> Canadian Bio-Inorganic Chemistry Conference, Parry Sound, Ontario. May 23, **2019**.

“The Effects of Trivalent Chromium on Single Live Cells using Scanning Electrochemical Microscopy” Jonathan M. Wong, Fraser P. Filice, Lina Yao, and Zhifeng Ding, 101<sup>st</sup> Canadian Chemistry Conference, Edmonton, Alberta. May 30, **2018**.